

Development of Highly Potent and Selective FGFR4 Inhibitors Based on S_NAr Electrophiles

Moritz Schwarz¹, Maksym Kurkunov^{1,2}, Florian Wittlinger¹, Ramona Rudalska^{2,3}, Guiqun Wang^{4,5,6}, Martin P. Schwalm^{4,5,6}, Alexander Rasch¹, Benedikt Wagner^{1,2}, Stefan Laufer^{1,2,7}, Stefan Knapp^{4,5,6}, Daniel Dauch^{2,3,7}, Matthias Gehringer^{1,2,*}.

¹ Department of Pharmaceutical/Medicinal Chemistry, Institute of Pharmaceutical Sciences, Eberhard Karls University Tübingen, 72076 Tübingen, Germany.

² Cluster of Excellence iFIT (EXC 2180) 'Image-Guided and Functionally Instructed Tumor Therapies', University of Tübingen, 72076 Tübingen, Germany.

³ Department of Medical Oncology and Pneumology, University Hospital Tübingen, Tübingen, Germany.

⁴ German Cancer Research Consortium (DKTK), German Cancer Research Center (DKFZ), Heidelberg, Germany.

⁵ Goethe-University Frankfurt, Structural Genomics Consortium (SGC), Buchmann Institute for Molecular Life Sciences, Max-von Laue Str. 15, 60438 Frankfurt am Main, Germany.

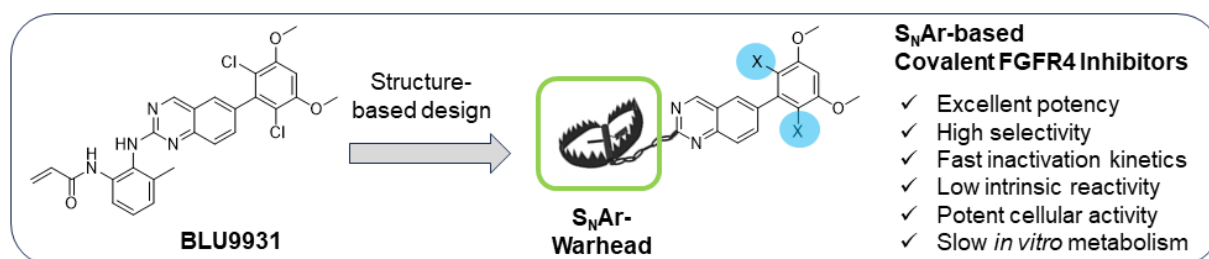
⁶ Goethe-University Frankfurt, Institute of Pharmaceutical Chemistry, Max-von Laue Str. 9, 60438 Frankfurt am Main, Germany

⁷ Tübingen Center for Academic Drug Discovery & Development (TüCAD₂), 72076 Tübingen, Germany.

* Correspondence: matthias.gehringer@uni-tuebingen.de; Tel.: +49-7071-29-74582

Abstract:

Fibroblast Growth Factor Receptor 4 (FGFR4) is thought to be a driver in several cancer types, most notably in hepatocellular carcinoma. One way to achieve high potency and isoform-selectivity for FGFR4 is to covalently target a rare cysteine (C552) in the hinge region of its kinase domain that is not present in other FGFR family members (FGFR1-3). Typically, this cysteine is addressed via classical acrylamide electrophiles. Here, we demonstrate that non-canonical covalent “warheads” based on nucleophilic aromatic substitution (S_NAr) chemistry can be employed in a rational manner to generate highly potent and (isoform-)selective FGFR4 inhibitors with a low intrinsic reactivity. Our key compounds showed low- to subnanomolar potency, efficient covalent inactivation, and excellent selectivity over other FGFRs as well as kinases with an equivalent cysteine and a representative subset of the kinome. Moreover, these compounds achieved low nanomolar potencies in cellular assays and demonstrated good microsomal stability highlighting the potential of S_NAr -based approaches in covalent inhibitor design.



Keywords: protein kinases, fibroblast growth factor receptor, covalent inhibitors, cysteine, structure-based design, nucleophilic aromatic substitution.

Introduction

The fibroblast growth factor receptor (FGFR) family is essential for many physiological processes such as cell growth and tissue repair while upregulation, e. g. through mutation, drives pathological processes that can ultimately lead to various types of cancer. [1–3] The FGFRs are receptor tyrosine kinases (RTKs) and the family consists of four members in humans, namely FGFR1-4, which are activated by the extracellular binding to fibroblast growth factors (FGFs). [4] Inhibition of FGFRs has proven to be a viable strategy for cancer therapy as highlighted by the approval of three non-covalent pan-FGFR inhibitors (Erdafitinib [5], Pemigatinib [6], and Infigratinib [7]) and one covalent inhibitor (Futibatinib (**1**) [8], see Figure 1) for the treatment of urothelial carcinoma (Erdafitinib) and cholangiocarcinoma (Pemigatinib, Infigratinib, Futibatinib). As a result of the aberrant signaling of its natural ligand FGF19, FGFR4 has been particularly associated with hepatocellular carcinoma (HCC), the most common type of hepatic cancer. [9, 10] The reason for the proliferative effects lies in the FGF19/FGFR4 signaling pathway, where FGF19 binds FGFR4 and its co-receptor β -Clotho leading to dimerization and autophosphorylation. Subsequently, the intracellular kinase domain of FGFR4 phosphorylates the FGFR substrate 2 (FRS2), which activates downstream signaling pathways such as the phosphoinositide 3-kinase (PI3K)/AKT or the mitogen-activated protein kinase (MAPK) pathway. [11, 12] All approved FGFR inhibitors either show inhibition of all FGFRs or are biased towards FGFR1-3 with less activity against FGFR4. [13] This unselective inhibition leads to unwanted side effects in the treatment of FGFR4-driven diseases that may require dose reduction and thereby reduce clinical efficacy. [13, 14] An example of such a dose-limiting side effect is the hyperphosphatemia often observed with FGFR1 inhibition due to the disruption of FGF23-mediated phosphate homeostasis. [15, 16] Therefore, it is of great interest to develop selective FGFR4 inhibitors to optimize the

efficacy in FGFR4-dependent pathologies while minimizing the side effects arising from FGFR1-3 inhibition.

Covalent inhibitors have recently experienced a renaissance in drug discovery and chemical biology where covalent approaches enabled the development of various kinase-targeted chemical probes and drugs. [17–21] Cysteine residues are particularly suited for being covalently addressed because of the nucleophilic character of their thiol(ate) side chain, which facilitates the reaction with weakly electrophilic groups (typically referred to as the “warhead”) to form a covalent bond. A common approach to achieve selectivity between closely related protein kinases is to covalently bind a poorly conserved cysteine that is unique to the family member of interest. [22, 23] This approach has been successfully exploited for several kinases such as PI3K α [24, 25], S6K2 [26], and JAK3 [27], and it enabled the development of the first approved isoform-selective JAK3 inhibitor Ritlecitinib (PF-06651600). [28, 29] While Futibatinib and other covalent pan-FGFR inhibitors address a cysteine in the P-loop that is conserved among all FGFR isoforms, a rational approach to achieve FGFR4 selectivity is provided by differences in the amino acid sequences in the FGFR hinge region: FGFR4 harbors a non-conserved cysteine (C552) at the middle-hinge region two positions C-terminal of the gatekeeper amino acid (GK+2 position) while the other three FGFRs have a tyrosine residue at this position (Figure 2A,B). [30] This cysteine, which is only shared by four other protein kinases (MAPKAPK2 (MK2), MAPKAPK3 (MK3), p70S6K β (S6K2), and TTK (MPS1)) (Figure 2B), [31] can be addressed covalently to specifically enhance potency on FGFR4 generating a selectivity window against the other FGFR isoforms. At the same time, the steric demand of the warhead may induce a steric clash with the larger tyrosine residue present in the other FGFRs to further enhance selectivity.

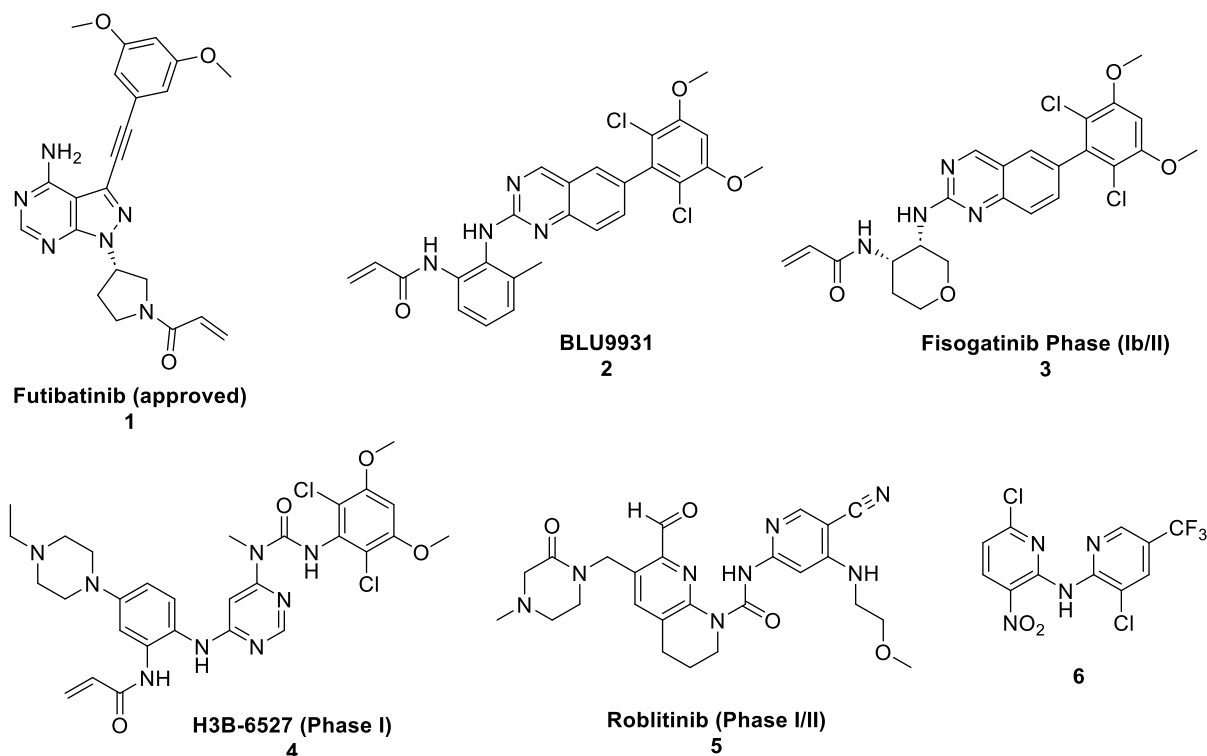


Figure 1: Structures of the approved covalent pan-FGFR inhibitor Futibatinib, covalent FGFR4 inhibitors in clinical trials, and compound **6** from Fairhurst *et al.* [30]

Covalent targeting of FGFR4-C552 by means of “classical” acrylamide warheads undergoing an irreversible (i.e. under physiological conditions and with respect to the protein’s half-life) thia-Michael addition reaction has been successfully applied by Hagel *et al.* who discovered the first-in-class covalent FGFR4 inhibitor **BLU9931 (2)** (Figure 1). [32] Subsequently, other groups developed Michael-acceptor-based FGFR4 inhibitors employing a variety of scaffolds (7-azaindoles [33], 1,6-naphthyridin-2(1*H*)-ones [34], aminoindazoles [35], 2-aminopyrimidines [36] and quinazolines [37, 38]) and these efforts culminated in the development of several inhibitors such as Fisogatinib (BLU-554, **3**) [39] and H3B-6527 (**4**) [40, 41] which have advanced to phase I and II clinical trials (Figure 1). Moreover, reversible covalent inhibitors based on aldehyde warheads forming a hemithioacetal adduct have been developed by

researchers from Novartis [42, 30] and others [43, 44], which led to the discovery of clinical candidate Roblitinib (FGF-401, **5**, see Figure 1). [45, 46]

An underexplored approach to covalently addressing cysteines involves warheads based on electron-deficient heteroaromatic rings equipped with a leaving group, which can react with nucleophiles via a nucleophilic aromatic substitution (S_NAr) reaction (see the mechanism in Figure 2C). [47] The general applicability of this approach to targeting FGFR4-C552 has been proven by Fairhurst *et al.*, who identified fragment-like chloronitropyridine-based inhibitor **6** in a high throughput screening (Figure 1). [30] However, this compound was not pursued further in favor of the reversible-covalent inhibitors mentioned above. Considering its small size, compound **6** showed a remarkable potency ($k_{inact}/K_I = 3.0 \cdot 10^4 \text{ M}^{-1} \text{ s}^{-1}$, $IC_{50} = 32 \text{ nM}$) and the covalent binding to C552 via S_NAr displacement at the chloronitropyridine has been confirmed by mass spectrometry, cysteine mutation and X-ray crystallography (PDB: 5NUD). Notably, a structurally equivalent cysteine is addressed in the protein kinase MAPKAPK2 (MK2) by the recently published S_NAr -based inhibitor CC-99677 which was developed for the treatment of autoimmune disorders and had entered clinical trials. However, this more elaborate compound, which relies on a 2-chloropyrimidine warhead, achieves a comparatively low efficiency of covalent inactivation ($4.9 \cdot 10^3 \text{ M}^{-1} \text{ s}^{-1}$, $IC_{50} = 156 \text{ nM}$ on MK2). [48]

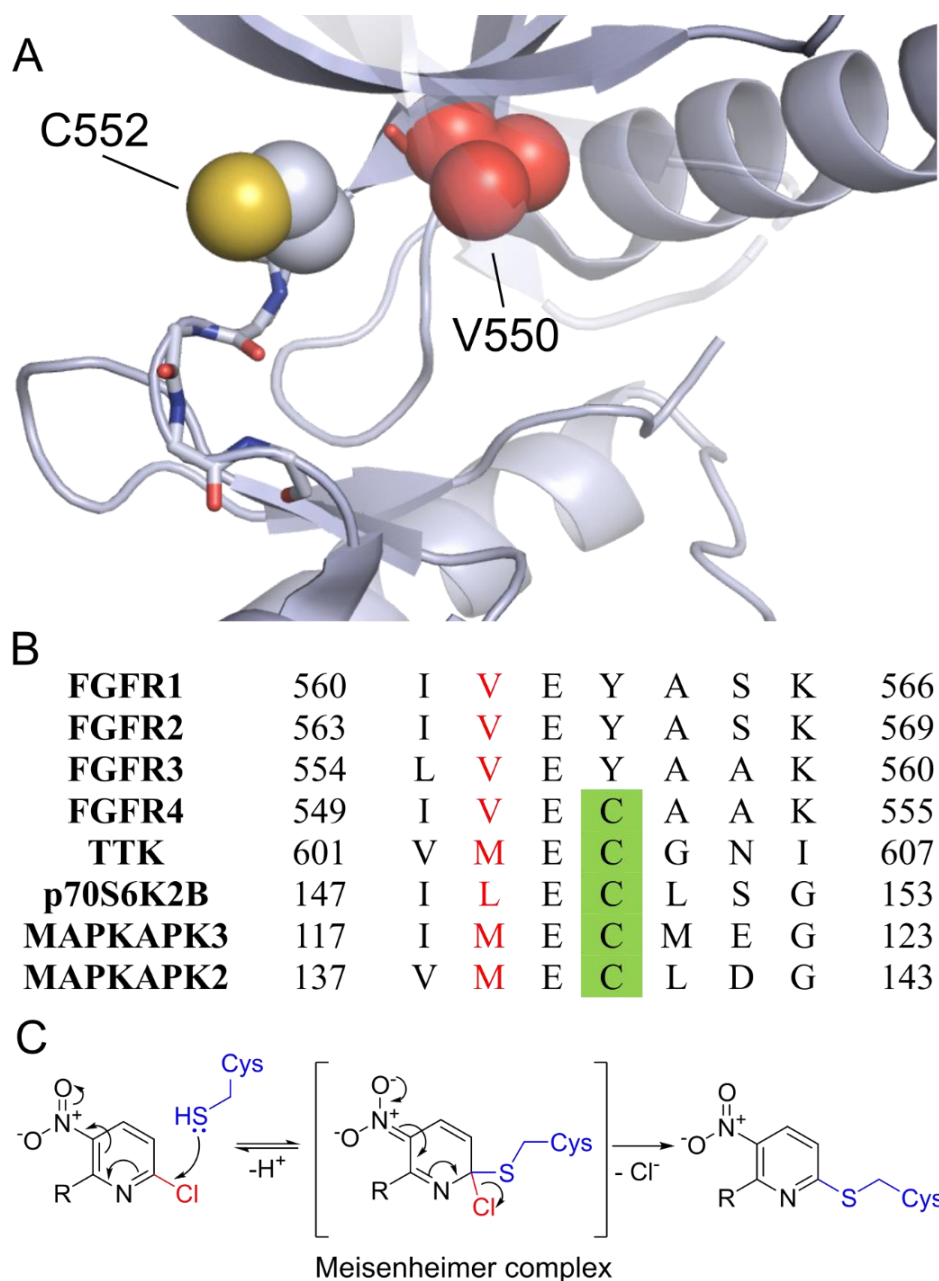


Figure 2: **A:** Position of C552 within the ATP pocket of the kinase domain of FGFR4. The hinge region is shown as sticks (PDB: 5NUD), the side chains of Cys552 and the gatekeeper (GK) Val550 (red) are highlighted as spheres. **B:** Sequence alignment of the hinge regions of the FGFR family and the other kinases containing a cysteine in the GK+2 position (highlighted in green). The GK residues are highlighted in red letters. **C:** Mechanism of an S_NAr reaction between a cysteine and a chloronitropyridine-warhead proceeding via a Meisenheimer complex.

The aim of the present work was to further explore the scope of S_NAr -based warheads for FGFR4 inhibition. To this end, we merged the well-established scaffold of **BLU9931** and related FGFR inhibitors, which confers high (non-covalent) affinity and selectivity

for the FGFR family, with different S_NAr warheads to investigate whether such a combination leads to highly potent and isoform-selective FGFR4 inhibitors (Figure 3A,D-F). Compared to the more common acrylamide warheads, S_NAr warheads show several potential advantages, most notably their broadly tunable reactivity which is adjustable via the electron deficiency of the (hetero)aromatic system and the leaving group. Moreover, the higher rigidity and geometric constraints of such electrophiles require a proper placement of the nucleophile to facilitate the reaction, which may allow to address the target nucleophile more selectively. Beyond this, electron-deficient heteroarenes typically show a good metabolic stability and in the simplest case only one hydrogen atom must be substituted from an electron deficient aromatic ring of an existing inhibitor to enable covalency, while the addition of an α,β -unsaturated requires an increase of at least 5 heavy atoms and simultaneously introduces polar groups, which are not always compatible with buried binding sites. [47]

Design:

The structural design of our study was based on the superimposition of two different covalent FGFR4 inhibitor complexes. One was with the isoform-selective inhibitor **BLU9931 (2)**, with an acrylamide warhead, and the other one was the fragment-like compound **6** from Fairhurst and colleagues with a chloronitropyridine S_NAr warhead (Figure 3A). Notably, we have previously employed a similar approach for the design of the first isoform-selective S6K2 inhibitor starting from the S6K1 inhibitor PF-4708671. [26] Examining the co-crystal structure of compound **6** revealed an interesting binding mode with the two pyridine nitrogen atoms forming hydrogen bonds (HBs) with the same NH group of the backbone of A553 in the hinge region (Figure

3B). While these hydrogen bonds are not equal, with the one formed by the S_NAr warhead's pyridine being longer and not ideally oriented, we hypothesize that a more ideal "chelate-like" binding mode may be present in the reversibly bound pre-reaction complex which would facilitate the entry of the nucleophile in an appropriate angle from above the aryl plane. Moreover, an intramolecular hydrogen bond between the NH of the biaryl amino linker and the nitro group in compound **6** may assist the proper pre-orientation of the electron-deficient heteroaryl system towards C552 (Figure 3B), which is also compliant with a similar hydrogen bond being observed in a small molecule X-ray crystal structure of a different chloronitropyridine-linked scaffold. [49]

BLU9931 is based on the widely used quinazoline scaffold, which is also present in several other FGFR inhibitors. [50] Here, the 2,6-dichloro-3,5-dimethoxy substituent attached to the 6-position of the quinazoline enhances potency and selectivity by properly occupying the hydrophobic pocket behind the valine gatekeeper residue (Val550) and one of the methoxy groups further forms a hydrogen bond towards the backbone of the conserved DFG motif (Figure 3C). [30, 51] The superposition of the crystal structure of compound **6** and **BLU9931** covalently bound to FGFR4-C552 shows how the hinge-binding pyridine ring of compound **6** overlays well with the pyrimidine ring of the **BLU9931** quinazoline suggesting that the chloronitropyridine warhead of compound **6** may be installed on the latter without significantly altering its positioning (Figure 3D). This hypothesis was further confirmed by covalent docking of the prototype hybrid compound **7B** (Figure 3E,F). The docking pose matches the expected binding mode, although it does not perfectly reproduce the planar arrangement of the pseudo-cyclic system resulting from the intramolecular NH-nitro hydrogen bond as observed in the co-crystal structure of compound **6**. As mentioned, we assume that this (presumably weak) intramolecular HB is important for pre-

orienting and potentially activating the compound in the binding site to achieve rapid target modification (Figure 4A), which would also be in line with the recently disclosed data on CC-99677 where such interaction is absent. We hypothesize that this may at least in part account for the relatively slow inactivation rates of the latter compound.

With the aim of corroborating this hypothesis, we also designed compounds devoid of this interaction. To prevent a potential disruption of the binding mode by “unmasking” the linker NH to present the common donor–acceptor hinge interaction pattern, [52] which would orient the warhead away from the target cysteine (see the schematic depiction in Figure 4A), we synthesized compounds which lacked a hydrogen bond donor (HBD) at the linker position. For this purpose, the amino linker was replaced by a sulfur linker as it is more flexible and synthetically more accessible compared to an analogous oxygen linker while covalent docking suggested similar interaction energies of both variants (see the docking poses in Figure S1 and S2). In compounds that lacked the nitro group, an additional nitrogen atom was incorporated into the warhead’s heteroarene to compensate for electron-withdrawing properties of the nitro group. As a possibility to reinforce the orientation imposed by the intramolecular NH–nitro HB, we further designed analogs where the orientation was frozen by means of a second ring, i.e. in a bicyclic quinazoline or 7*H*-pyrrolo[2,3-*d*]pyrimidine, which were directly *C*- or *N*-linked to the core scaffold (see Figure 4B and the docking poses in Figure S3 and S4).

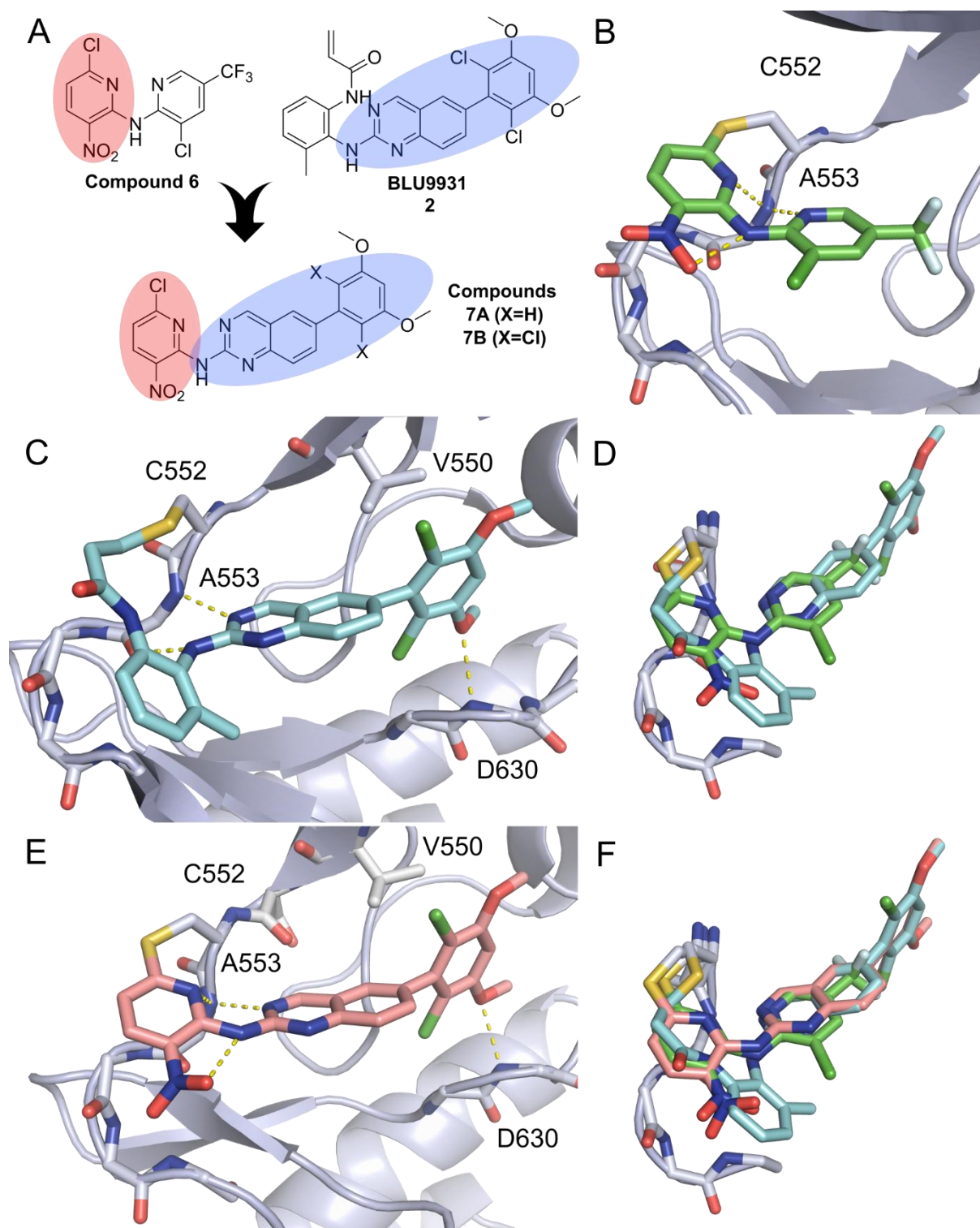


Figure 3: **A)** Compound **6** from Fairhurst et al. with its S_NAr -warhead highlighted in red, **BLU9931** with the FGFR-binding scaffold highlighted in blue. The structural combination of both moieties is illustrated underneath resulting in compounds **7A/B**. **B)** Compound **6** covalently interacting with C552 (PDB: 5NUD). The intramolecular HB and the chelate-like HBs are shown as dotted yellow lines. Key residues C552 and A553 are shown as sticks. **C)** **BLU9931** covalently interacting with C552 (PDB: 4XCU). The HBs to hinge region and D630 of the DFG motif are shown as dotted yellow lines. **D)** Overlay of the above-mentioned crystal structures of compound **6** (green) and **BLU9931** (blue). Only the hinge region of the protein is displayed for clarity. **E)** Docking pose of compound **7B** covalently bound to C552. **F)** overlay of compound **6**, **BLU9931** and the covalent docking pose of compound **7B**.

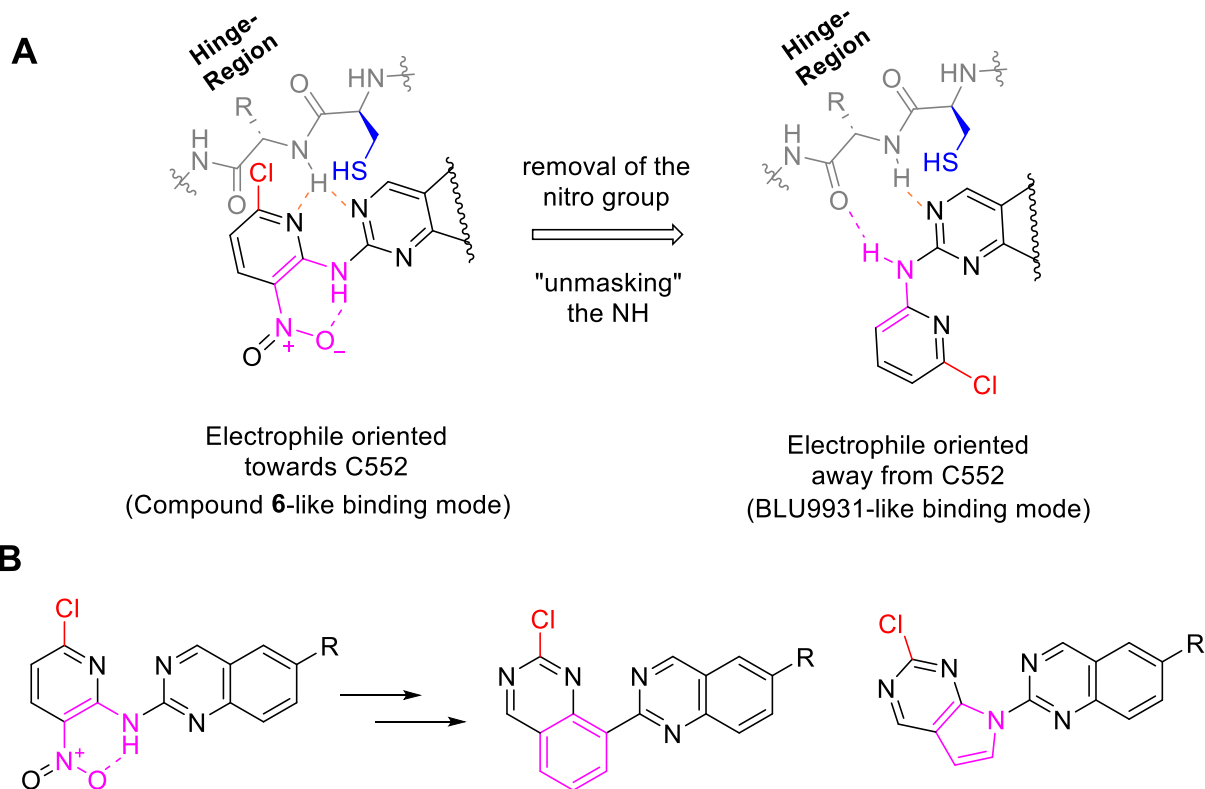


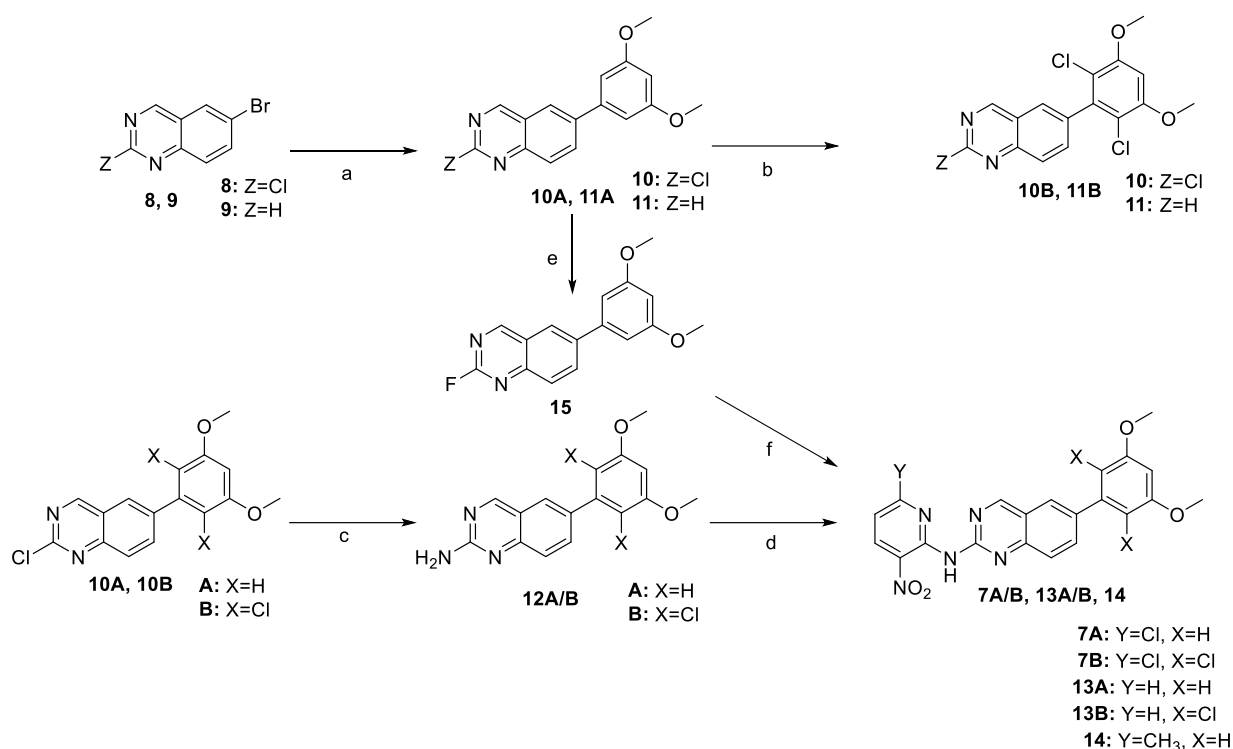
Figure 4: **A)** “Unmasking” of the linker NH to present a donor–acceptor hinge binding motif orienting the warhead away from the target cysteine. **B)** Freezing of the orientation imposed by the NH–nitro HB (magenta) by cyclisation (magenta) leads to bicyclic C–C and C–N-linked warheads. The leaving group of the warheads is colored in red.

Synthesis:

The synthesis of inhibitors **7A/B**, **11A/B**, **13A/B** and **14** is schematically shown in Scheme 1. It starts with a Suzuki cross-coupling reaction of 6-bromoquinazolines **8** and **9** with 3,5-dimethoxyphenylboronic acid at room temperature under previously optimized conditions using tri-*tert*-butylphosphine-ligated Pd⁰ generated from the respective 3rd generation Buchwald pre-catalyst. [53, 54] The following chlorination of the electron-rich dimethoxyphenyl system in the obtained intermediates **10A** and **11A** was carried out by the addition of sulfuryl chloride in acetonitrile (ACN) at -20 °C in a moderate to very high yield. [55] Amination of the quinazolinone scaffold of 2-chloroquinazolines **10A** and **10B** was achieved by treatment with aqueous ammonia solution in 1,4-dioxane in a microwave reactor at 100 °C in a very high yield. Finally,

the S_NAr warheads were introduced by copper(I)-promoted Ullmann coupling of 2-aminoquinazolines **12A/B** with 2-bromo-6-chloro-3-nitropyridine using *trans*-1,2-diaminocyclohexane as the ligand. [56] Non-reactive analogue **13B** lacking the chloride leaving group at the nitropyridine was synthesized from 2-aminoquinazoline **12B** under equivalent Ullmann coupling conditions using 2-bromo-3-nitropyridine. In contrast, non-reactive control compounds **13A** and **14** (leaving group replaced by H and Me, respectively) were synthesized from aminoquinazoline **12A** via Buchwald-Hartwig coupling with the respective 2-bromopyridines using Pd₂(dba)₃ and XantPhos as the catalyst system. Due to the low yields, we further elaborated an alternative synthetic access to inhibitor **7A**. Starting from intermediate **10A** the quinazoline 2-chloro substituent was displaced by fluoride using Me₄NF**t*-amyl alcohol in DMSO at room temperature. [57] The resulting 2-fluoroquinazoline derivative **15** was reacted with 6-chloro-3-nitropyridin-2-amine in an S_NAr reaction to obtain compound **7A**.

Scheme 1: Synthesis of the compounds 7-14

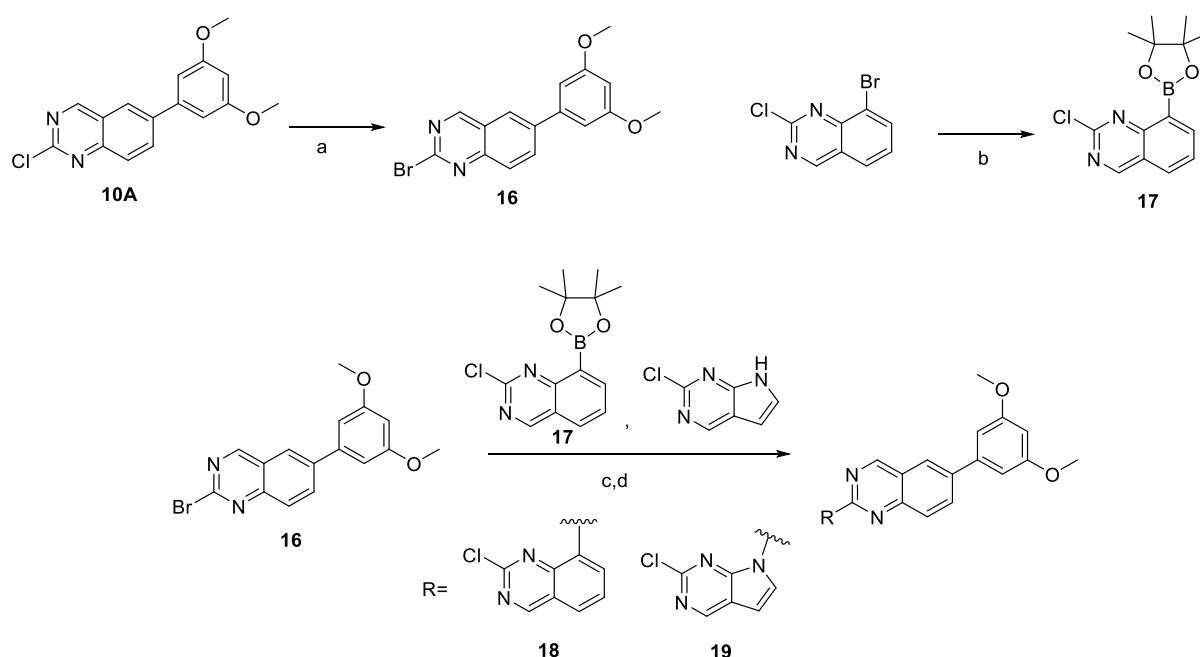


Reagents and conditions are as follows: **a**: (3,5-dimethoxyphenyl)boronic acid, potassium phosphate, $P(t\text{-butyl})_3\text{Pd G3}$, 1,4-dioxane, H_2O , RT, **10A** (quant.) or **11A** (47%); **b**: sulfuryl chloride, ACN, $-20\text{ }^\circ\text{C}$, **10B** (quant.) or **11B** (35%); **c**: NH_3 (aq.) 20%, 1,4-dioxane, MW, $100\text{ }^\circ\text{C}$, **12A** (quant.) or **12B** (93%); **d**: to obtain **7A/B** and **13B**: 2-bromo-6-chloro-3-nitropyridine or 2-bromo-3-nitropyridine, potassium carbonate, copper(I) iodide, *trans*-1,2-diaminocyclohexane, 1,4-dioxane, $90\text{ }^\circ\text{C}$, 7 h, **7A** (9%), **7B** (12%), or **13B** (13%). To obtain **13A** and **14**: 2-bromo-3-nitropyridine or 2-bromo-6-methyl-3-nitropyridine, cesium carbonate, $\text{Pd}_2(\text{dba})_3$, XantPhos, 1,4-dioxane, $100\text{ }^\circ\text{C}$, 18 h. **13A** (30%) or **14** (18%); **e**: $\text{Me}_4\text{NF}^+\text{t-amylalcohol}$, DMSO, RT, 18 h (54%); **f**: 6-chloro-3-nitropyridin-2-amine, Cs_2CO_3 , DMF, RT, 18 h, **7A** (30%).

For testing alternative warheads, we decided to proceed with the series lacking the dichloro substitution at the phenyl ring, since this reduces the chemical complexity and the likelihood of solubility issues, while the scaffold maintains sufficient (non-covalent) FGFR affinity to derive useful structure–activity relationships (SAR). [33] To facilitate the following cross-coupling reactions, the synthesis of final compounds **18** and **19**, which have a bicyclic warhead, started with a chloride-to-bromide displacement of 2-chloroquinazoline intermediate **10A** by means of bromotrimethylsilane under reflux in propionitrile (Scheme 2). [58] For the synthesis of compound **18** featuring a 2-chloroquinazoline warhead, the 8-bromo-2-chloroquinazoline precursor was first

converted into the corresponding 8-pinacol boronate ester (**17**) via Miyaura borylation [59] and then cross-coupled with 2-bromoquinazoline **16** under the aforementioned mild Suzuki conditions. Compound **19** with a 2-chloro-7*H*-pyrrolo[2,3-*d*]pyrimidine warhead was prepared from bromoquinazoline **16** and the corresponding pyrrolopyrimidine in a copper catalyzed Ullmann reaction (*vide supra*).

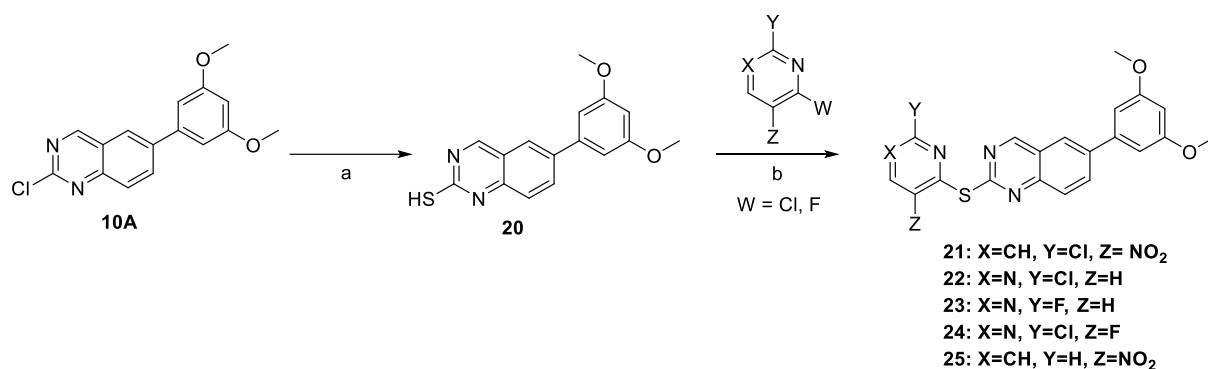
Scheme 2: Synthesis of the compounds 18 and 19



Reagents and conditions are as follows: **a**: bromotrimethylsilane, propionitrile, reflux, (31%); **b**: bispinacolatodiborane, Pd(dppf)Cl₂, potassium acetate, 1,4-dioxane, 95°C, 4h; **c**: potassium phosphate, P(*t*-butyl)₃ Pd G3, 1,4-dioxane, H₂O, RT, (31%); **d**: potassium carbonate, copper(I) iodide, *trans*-1,2-diaminocyclohexane, 1,4-dioxane, 100 °C, (57%).

In addition to amino-linked and bicyclic warheads, compounds with a sulfur linkage between the warhead and the quinazoline scaffold were prepared (Scheme 3). To this end, 2-chloroquinazoline **10A** was refluxed in ethanol with thiourea yielding an intermediate 2-thiuronium salt via S_NAr displacement of the chloride. After precipitation, hydrolysis with 0.1 N sodium hydroxide solution gave 2-mercaptoquinazoline **20**. Final compounds **21-25** were subsequently synthesized via S_NAr reaction of thiol **20** with a selection of fluoro- and chloropyri(mi)dines.

Scheme 3: Synthesis of the compounds 21-25



Reagents and conditions: **a**: 1) thiourea, ethanol, reflux, 48 h, 2) NaOH 0.1 N, ethanol, RT, (48%); **b**: potassium-*tert*-butoxide, THF, RT, **21** (57%), **22** (53%), **23** (79%), **24** (63%), or **25** (20%).

Results and discussion

Biochemical and biophysical evaluation

For the evaluation of our FGFR4 inhibitors, we initially tested all compounds in the HotSpot™ format, a radiometric protein kinase enzyme assay. [60] In line with our design hypothesis, prototype compound **7B** and its derivate **7A** lacking the phenyl dichloro substitution both showed very high potency for FGFR4 with (apparent) IC₅₀ values below the lowest tested concentration (i.e. IC₅₀ < 0.5 nM in both cases; see Table 1). Notably, the intrinsic reactivity of prototype **7B** was low as shown by an almost 5-fold longer half-life compared to the approved covalent kinase inhibitor afatinib in a GSH stability assay (see Table S1). These compounds were further re-tested and compared with **BLU9931** in a complementary continuous kinase assay format (PhosphoSens®) relying on the phosphorylation of a CSox peptide. [61] Again, all compounds showed excellent inhibitory potencies with compound **7B** (IC₅₀ = 1.2 nM) being slightly more potent than **BLU9931** (IC₅₀ = 2.0 nM) while analog **7A** was slightly less potent (IC₅₀ = 4.5 nM).

As expected, the corresponding non-reactive control compounds lacking the chloride leaving group (**13A/B**) showed only weak activity with the dichloro dimethoxyphenyl

analog **13B** being slightly more active ($IC_{50} = 1.7 \mu M$) than the non-chlorinated analog **13A** ($IC_{50} > 5 \mu M$). To exclude the possibility that the differences in inhibitory activity between the compounds with and without the chloride leaving group arose solely from the steric properties of the pyridine 2-chloro substituent, we synthesized 2-methyl analog **14** which was also poorly active ($IC_{50} \gg 5 \mu M$). This supports the notion of a covalent mode-of-action of inhibitors **7A** and **7B** which both show a dramatically increased potency. To gain more insights in the reversible binding contribution of the *N*-linked nitropyridine, we also tested analogs **11A** (di-OMe-Ph) and **11B** (di-Cl-di-OMe-Ph) completely devoid of the nitropyridine fragment. While compound **11A** (di-OMe-Ph) again had an IC_{50} value above the highest concentration tested ($> 5 \mu M$), compound **11B** with the di-Cl-di-OMe-phenyl residue showed a similar activity ($IC_{50} = 2.1 \mu M$) as its nitropyridine-substituted analog **13B**, suggesting a relatively neutral contribution of the *N*-linked nitropyridine fragment to binding affinity.

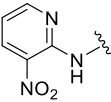
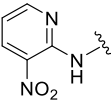
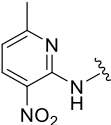
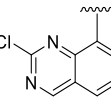
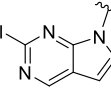
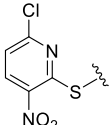
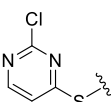
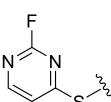
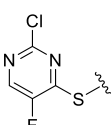
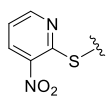
Assessment of the compounds with rigid bicyclic warheads that were directly C–C- or C–N-linked revealed an enormous decrease in inhibitory activity for both, compound **18** ($IC_{50} \sim 5 \mu M$, 54 % residual activity at $5 \mu M$) and compound **19** ($\gg 5 \mu M$) compared to our amine-linked chloronitropyridine prototype compounds. Possible reasons for this include a non-ideal pre-orientation towards C552 imposed by the lack of flexibility, an insufficient intrinsic reactivity, and the low solubility imposed by their highly planar and lipophilic nature, which may have compromised IC_{50} determination and also hampered the assessment of intrinsic reactivity in a GSH stability assay.

Sulfur-linked compounds also showed poor inhibitory activity. While a low potency of non-reactive analog **25** ($IC_{50} \gg 5 \mu M$) was not unexpected, the weak performance of the reactive 2-chloro and 2-fluoro pyrimidine analogs **22-24** was more surprising. While the most reactive among these compounds, chloronitropyridine **21**, with a 2-fold lower

GSH half-life compared to Afatinib, showed an IC_{50} of 4.5 μ M, the IC_{50} values of all other compounds were found to be > 5 μ M. The GSH half-life of the S-linked 2-fluoropyrimidine (**23**) was in the same range as the one of prototype compound **7B**, and the analogous 2-chloro-5-fluoropyrimidine (**24**) showed a significantly enhanced reactivity even higher than the one of Afatinib, indicating that insufficient intrinsic reactivity is not the cause of the low potency of these compounds. Possible reasons may be found in differences in the spatial extension and bond lengths/geometries of the sulfur linker that might cause a suboptimal orientation of the warhead towards the thiol group of the cysteine as well as the high flexibility and lack of the intramolecular hydrogen bond further impeding a proper pre-orientation for the entry of the nucleophile.

Table 1: SAR of the different 2-substituted quinazoline-derivates

Compound	X	R	Biochemical IC_{50} (nM)	
			FGFR4	
BLU9931	Cl		N.D. ^a	2.0 ^b
7A	H		< 0.5 ^a	4.5 ^b
7B	Cl		< 0.5 ^a	1.2 ^b
11A	H	H	>5000 ^a	
11B	Cl	H	2090 ^a	

13A	H		>5000 ^a
13B	Cl		1700 ^a
14	H		>5000 ^a
18	H		>5000 ^a
19	H		>5000 ^a
21	H		4450 ^a
22	H		>5000 ^a
23	H		>5000 ^a
24	H		>5000 ^a
25	H		>5000 ^a

^aKinase activity assays were commercially conducted at ReactionBiology Corp. using a HotSpot™ assay at an 10 μM ATP concentration. ^bKinase activity was commercially determined at AssayQuant using the PhosphoSens® CSox-based continuous assay format at K_M ATP. N.D.: not determined

Beyond potency, selectivity of protein kinase inhibitors is of major importance as limited selectivity may result in side effects and toxicities. As discussed above, we placed particular emphasis on the off-target activity inside the FGFR family. Moreover, covalent inhibitors tend to have off-target (re)-activities towards kinases

with equivalently positioned cysteines, i.e. with a GK+2 cysteine in the case of FGFR4. Therefore, our key compounds **7A** and **7B** were tested in the HotSpot™ format [60] against all other FGFRs as well as MAPKAPK2, MAPKAPK3, S6K2, and TTK harboring a GK+2 cysteine (Table 2). Both compounds were highly selective within the FGFR family with compound **7B** showing weak inhibitory activity for FGFR1 (IC₅₀ = 4.4 μM) and FGFR2 (IC₅₀ = 490 nM) while all other IC₅₀ values were above 5 μM. Selectivity against MAPKAPK2, MAPKAPK3, and TTK was also excellent as none of these kinases showed an IC₅₀ below 5 μM. However, compound **7A** showed pronounced off-target activity on S6K2 (IC₅₀ = 4.5 nM) while compound **7B** was highly selective (IC₅₀ = 1.8 μM). The reason for these varying selectivity profiles might be related to the more pronounced out-of-plane torsion of the phenyl ring caused by two *ortho*-chloro substituents as well as a steric clash of the latter with the larger leucine gatekeeper residue in S6K2 (see the alignment in Figure 2B), which is also in agreement with the loss of activity of Fisogatinib (**3**) against the FGFR4 V550L gatekeeper mutant.[62]

Table 2: Selectivity of compound 7A and 7B against other FGFR family members and kinases with a GK+2 cysteine.

Compound	FGFR1 [nM]	FGFR2 [nM]	FGFR3 [nM]	FGFR4 [nM]	S6K2 [nM]	MAPKAPK2 [nM]	MAPKAPK3 [nM]	TTK [nM]
7A	>5000	>5000	>5000	<0.5	4.48	>5000	>5000	>5000
7B	4370	490	>5000	<0.5	1820	>5000	>5000	>5000

Inhibitory activities were commercially determined at ReactionBiology Corp. using a HotSpot™ assay at 10 μM ATP concentration.

To assess the selectivity of our lead compounds **7B** and **7A** in a wider kinome context, we screened these inhibitors against 104 kinases with a broad distribution in the kinome using a differential scanning fluorimetry based assay (thermal shift assay) (Table S4). [63] To distinguish between effects related to covalent binding from such

residing on non-covalent interactions, we further included non-reactive analog **13B** as a control. To our delight, all tested compounds showed an exquisitely clean profile within the tested subset of the kinome. Compound **7A** showed the highest selectivity in this panel as it only affected the bromodomain TIF1A, a frequent off-target of kinase inhibitors [64], with a thermal shift slightly above 2 °C while no significant shift was observed for the other members of the FGFR family (FGFR4 was not included in this panel). In line with their higher affinity reversible FGFR binding element, compound **7B** and control **13B** showed a more pronounced thermal stabilization of FGFR1, 2 and 3 with the highest thermal shift to FGFR3 ($\Delta T_m = 7.9$ °C and 4.5 °C, respectively). However, as our IC₅₀ data demonstrated, this moderate thermal stabilization did not translate into a substantial inhibition of FGFR3 kinase activity.

While the above data was coherent with a covalent mode-of-action, it did not directly prove the formation of the covalent bond via S_NAr displacement. Thus, we performed intact protein mass spectrometry measurements of FGFR4 upon incubation with inhibitors **7A** and **7B**. Both compounds showed virtually complete labeling after 2 h incubation with the expected mass shift of the recombinant kinase domain of 401 Da and 472 Da for compounds **7A** and **7B**, respectively, which is consistent with the loss of a chloride. For compound **13B** we observed no mass shift which is consistent with its inability to undergo S_NAr reaction to form a covalent bond.

Evaluation of binding kinetics

Time dependence of potency is hallmark of covalent inhibitors which has led to different sets of criteria which should be applied for their evaluation and publication. [65–67] Most notably, covalent inhibitors typically act via a non-equilibrium 2-step binding mechanism, where an initial reversible binding event is followed by the formation of a covalent bond. As a consequence, the potency of covalent inhibitors expressed as IC₅₀

values increases over time. Covalent inhibitors are thus best described by a time-independent measure of potency, namely the second-order kinetic constant $k_{\text{inact}}/K_{\text{I}}$. [18, 17, 67] It is composed of the K_{I} value, which is the concentration where the rate of covalent bond formation becomes half maximal thus representing the non-covalent binding contribution. The 1st order rate constant k_{inact} , i.e. the maximal rate of covalent inactivation, describes how efficiently the covalent bond is formed from the pre-reaction complex. Importantly, k_{inact} is not necessarily correlated with intrinsic chemical reactivity since it is also impacted by pre-orientation to favor a low activation energy reaction trajectory and a possible activation of the electrophile by its non-covalent interactions with the target.

Since the determination covalent binding kinetics is relatively labor and resource intensive, it is common practice in the kinase field to perform early compound profiling by IC_{50} values determined under equivalent conditions while key compounds are subjected to kinetic profiling. Thus, we determined K_{I} , k_{inact} , and the $k_{\text{inact}}/K_{\text{I}}$ values of our lead compounds **7A** and **7B** and reference compound **BLU9931**. To this end, the compounds were tested in the aforementioned continuous assay format (PhosphoSens®) and kinetic parameters were derived from reaction progress curves at 24 different inhibitor concentrations. All tested inhibitors were efficient covalent binders with the same ranking as in the previously determined IC_{50} values, i.e. compound **7B** ($k_{\text{inact}}/K_{\text{I}} = 2.32 \cdot 10^5 \text{ M}^{-1} \cdot \text{s}^{-1}$) showed improved potency compared to **BLU9931** ($k_{\text{inact}}/K_{\text{I}} = 1.26 \cdot 10^5 \text{ M}^{-1} \cdot \text{s}^{-1}$) while the activity of unchlorinated derivative **7A** was slightly lower ($k_{\text{inact}}/K_{\text{I}} = 4.47 \cdot 10^4 \text{ M}^{-1} \cdot \text{s}^{-1}$). Differences of the obtained values appear to be primarily driven by the different K_{I} values (note that K_{I} does not equal the equilibrium binding constant K_{i}), with compound **7B** exhibiting the lowest K_{I} (5.7 nM vs. 38 nM and 14 nM for compound **7A** and **BLU9931**, respectively). These findings were

in agreement with previous observations showing that the dichloro-dimethoxyphenyl-substituted scaffold has a higher non-covalent binding affinity to FGFR4 than its unchlorinated counterpart. Interestingly, the k_{inact} values are almost the same for all tested compounds ($1.3\text{--}1.7 \times 10^{-3} \text{ s}^{-1}$), independent on whether an $\text{S}_{\text{N}}\text{Ar}$ -based or an acrylamide warhead is used. Moreover, the values are in the same range as the k_{inact} values of the FDA-approved EGFR inhibitors Afatinib ($0.9 \times 10^{-3} \text{ s}^{-1}$ on WT EGFR) [68] and Osimertinib ($36 \times 10^{-3} \text{ s}^{-1}$ on WT EGFR) [69] highlighting the potential of weakly reactive $\text{S}_{\text{N}}\text{Ar}$ electrophiles as replacements for the classical acrylamide warheads.

Table 4: results of kinetical study for the covalent inhibitors

Compound	K_{i} (nM)	k_{inact} (s^{-1})	$k_{\text{inact}}/K_{\text{i}}$ ($\text{M}^{-1}\cdot\text{s}^{-1}$)
7A	37.9±1.78	$1.7 \times 10^{-3} \pm 6.6 \times 10^{-5}$	$4.47 \times 10^4 \pm 420$
7B	5.7±0.17	$1.3 \times 10^{-3} \pm 3.1 \times 10^{-5}$	$2.32 \times 10^5 \pm 2.2 \times 10^3$
BLU9931	13.5±0.46	$1.7 \times 10^{-3} \pm 4.8 \times 10^{-5}$	$1.26 \times 10^5 \pm 950$

The reaction kinetics were commercially determined at AssayQuant Technologies Inc. using the PhosphoSens® CSox-based kinetic assay format.

Evaluation of cellular activity and target engagement

To prove the intracellular target engagement and isoform-selectivity of our inhibitors, we tested key compounds **7A** and **7B**, non-reactive control **13B** and reference compound **BLU9931** in a NanoBRET assay against all FGFR isoforms. As expected, **7A**, **7B** and **BLU9931** showed potent cellular FGFR4 target engagement all with similar IC_{50} values in the double-digit nanomolar range. In contrast, a significantly lower potency was observed for non-reactive control **13B** ($\text{IC}_{50} = 2.26 \mu\text{M}$) in agreement with its strongly reduced activity in biochemical assays due to the lack of potency enhancement by covalent binding. A pronounced selectivity of the covalent inhibitors against all other FGFR isoforms was observed. In FGFR1-3, the reactive inhibitor **7B** showed similar, low micromolar IC_{50} values as its non-reactive analog **13B** suggesting

that the chloro substituent at the pyridine ring does not substantially impact non-covalent binding affinity. In this format, the highest isoform-selectivity was observed for compound **7A** were all IC_{50} values on FGFR1-3 were above 10 μ M, which aligns well with the data from the biochemical kinase assays (Figure 5A).

To test the activity of our inhibitors in FGFR4-dependent cells, we further assessed the antiproliferative effect of the above compounds in Hep3B cells (Figure 5B). [32] While control compound **13B** again showed only weak effects with an EC_{50} of more than 1 μ M, the covalently binding analogues **7A** and **7B** both showed very good antiproliferative activity with EC_{50} 's of 22 nM and 5 nM, respectively. Notably, the performance of both compounds was significantly better than the one of the reference compound **BLU9931** (EC_{50} = 62 nM).

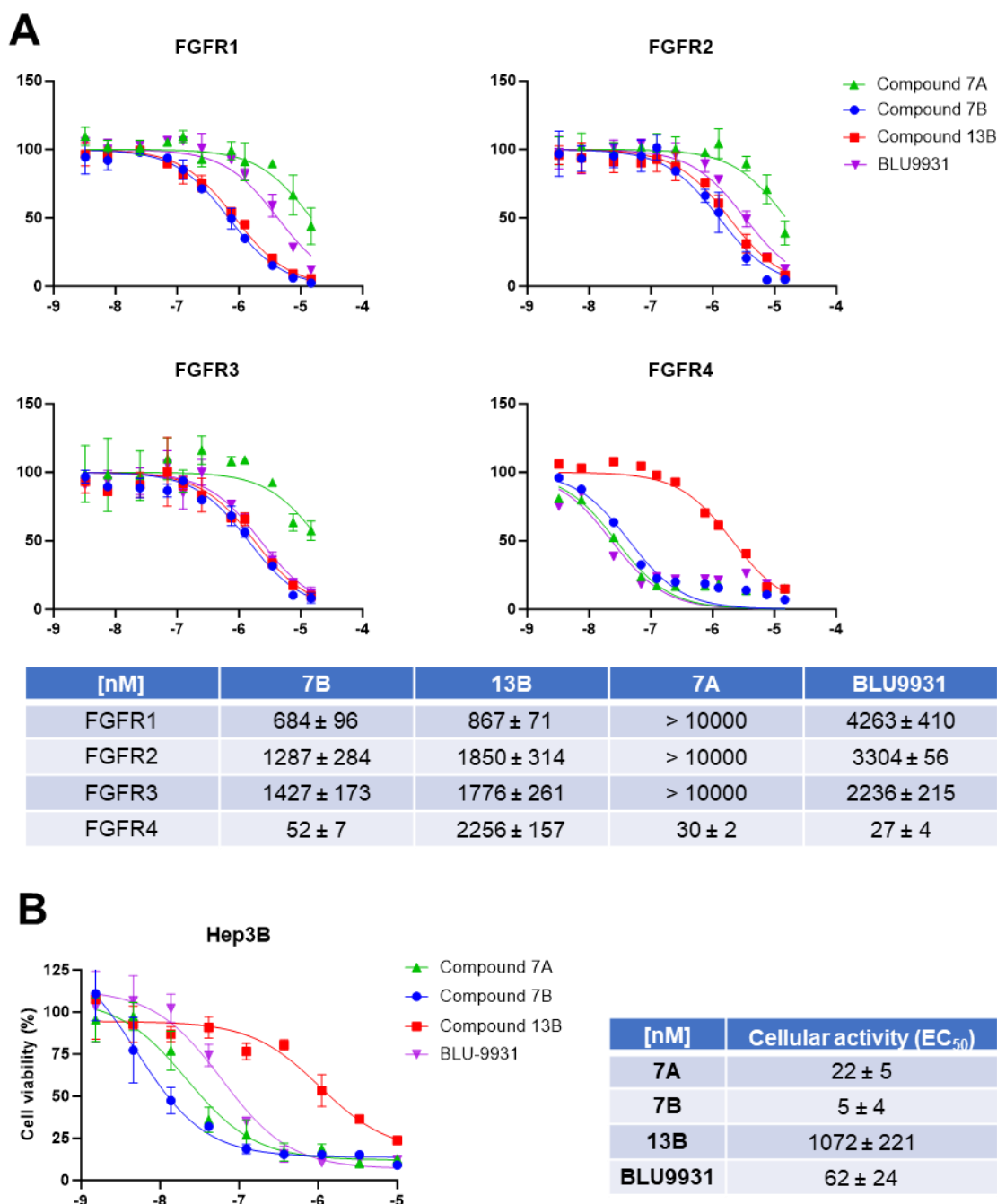


Figure 5: **A**: Intracellular target engagement of the compounds **7A**, **7B**, **13B** and **BLU9931** determined for the individual FGFR isoforms in a NanoBRET assay system. **B**: Cellular activity (EC₅₀) of the above FGFR4 inhibitors and the non-reactive control in the FGFR4-dependent Hep3B cell line.

Evaluation of metabolic stability in vitro

To learn more about the metabolic stability of our lead compound and to assess whether the S_NAr-warhead represents a metabolic soft spot, we monitored conversion of inhibitor **7B** and non-reactive analog **13B** by human liver microsomes (Figures S5,

S6). Both compounds were relatively stable with > 80% of unmetabolized compound remaining after 2 hours. The major metabolic transformation observed was oxidative demethylation of one methoxy group of the dimethoxyphenyl residue. Furthermore, we observed an additional metabolite for compound **7B** with an increased mass of 16 Da, which we assume to be the monohydroxylated hemiacetal precursor to the aforementioned demethylated metabolite, although no validation of this hypothesis has been performed and *N*-oxidation would also be a possible metabolic transformation with the same mass shift. Ultimately, we were pleased to see that the S_NAr warhead does not suffer from substantial metabolic transformation by microsomal enzymes.

Summary and conclusions

In summary, we designed a series of compounds with different S_NAr-based covalent warheads to target the protein kinase FGFR4. We established synthetic strategies to introduce *N*- and *S*-linked halopyri(mi)dine as well as bicyclic 2-chloroquinazoline and 2-chloro-7*H*-pyrrolo[2,3-*d*]pyrimidine electrophiles to the quinazoline-based scaffold of FGFR4 inhibitor **BLU9931**. Our key compounds **7A** and **7B** proved to be highly potent covalent FGFR4 inhibitors while other warheads led to substantially less active compounds suggesting that a proper combination of pre-orientation and reactivity is key to enable an efficient reaction with the target cysteine. We confirmed the covalent modification of FGFR4 with these compounds by mass spectrometry and the detected mass shift was compliant with the presumed S_NAr mechanism. Both key compounds showed efficient target inactivation with **7B** possessing almost 2-fold enhanced inactivation kinetics compared to the prototypical acrylamide-based covalent FGFR4 inhibitor **BLU9931**. Notably, the 1st order rate of covalent bond formation (k_{inact}) was on par with the one of the reference **BLU9931**'s acrylamide warhead despite the low

intrinsic reactivity of the chloronitropyridine S_NAr electrophile. The reactivity of the latter was substantially lower compared to the α,β -unsaturated amide of the approved covalent reference inhibitor Afatinib in a GSH assay. Moreover, our key compounds showed high selectivity over the other FGFR isoforms in both, cells (shown by NanoBRET) and biochemical assays. An exceptionally clean profile was observed for both compounds as well as unreactive control compound **13B** in a DSF-based kinome panel. We further showed the excellent selectivity of compound **7B** against the four other kinases with an equivalent cysteine. In contrast, **7A** also inhibited S6K2 which features the same cysteine but a bigger leucine gatekeeper. The activity of **7A** on S6K2 can be rationalized by the lower steric demand of the dimethoxyphenyl moiety occupying the behind-gatekeeper pocket compared to its dichloro-dimethoxy counterpart. We hypothesize that compound **7A** may therefore also retain its activity towards the FGFR4-V550L drug resistance mutant. In a cell viability assay using the FGFR4-dependent Hep3B cell line, both of our key compounds outperformed **BLU9931** with EC₅₀ values in the single digit nanomolar range for inhibitor **7B**. In addition, analysis of metabolic stability in human liver microsomes shows that the nitrochloropyridine warhead is not a metabolic soft spot encouraging the further exploration of S_NAr-based warheads in drug discovery.

Taken together, our results highlight that S_NAr-based covalent warheads can be installed to established scaffolds in a rational manner to generate highly potent and selective small molecule inhibitors with tempered reactivity, high labelling efficiencies and good metabolic stability. Moreover, our SAR data are in agreement with the suggested important role of the nitro group and its intramolecular hydrogen bond with the linker NH for targeting GK+2 cysteines, providing a rationale for further investigations. While the fully rigidified analogs employed in this study to mimic the

pseudo-bicyclic arrangement stabilized by this hydrogen bond did not show the desired activity, it will be important to explore whether more druglike hydrogen bond acceptor motifs may be employed in this context – possibly in combination with additional electron withdrawing substituents – to replace the nitro function while maintaining a proper combination of efficient target inactivation, low intrinsic reactivity and appropriate physicochemical properties.

Experimental selection

Chemistry. All starting materials and reagents were of commercial quality and were used without further purification. Dry and degassed solvents were used where indicated. Thin layer chromatography (TLC) was carried out on ALUGRAM® Xtra SIL G/UV254 silica plates (Macherey-Nagel, Düren, Germany) and visualized under UV light (254 nm and 366 nm). Preparative column chromatography was carried out with an Interchim PuriFlash 430 or PuriFlash XS420 (Interchim S.A., Montluçon, Allier, France) automated flash chromatography system using normal phase Grace Davison Davisil LC60A 20–45 micron silica (W.R. Grace and Company, Columbia, MD, USA) or Merck Geduran Si60 63–200 micron silica (Merck KGaA, Darmstadt, Germany).

Nuclear magnetic resonance (NMR) spectral analysis was performed on a Bruker Avance III HD 400 instrument (Bruker Corporation, Billerica, MA, USA). The samples were dissolved in deuterated solvents and chemical shifts were given in relation to tetramethylsilane (TMS). The multiplicity of signals was indicated with s = singlet, d = doublet, dd = doublet of doublets, t = triplet, q = quartet and m = multiplet. Spectra were calibrated using the residual proton peaks or the ^{13}C peaks of the used solvent.

Mass spectrometry (MS) was carried out with an Advion TLC-MS interface (Advion, Ithaca, NY, USA) with electrospray ionization (ESI) in positive and/or negative mode. Instrument settings were as follows: ESI voltage 3.50 kV, capillary voltage 187 V, source voltage 44 V, capillary temperature 250 °C, desolvation gas temperature 250 °C, and gas flow 5 L/min nitrogen. HR-MS measurements were performed at the mass spectrometry department, Institute of Organic Chemistry, Eberhard-Karls-University Tübingen.

HPLC purity was determined on an Agilent 1100 system (degasser, binary pump, injection module and ColCom setup, Agilent Technologies Inc., Santa Clara, CA, USA) with a DAD detector module (detection at 254 nm and 230 nm wavelength). The HPLC method for purity assessment was as follows: Method A: Phenomenex Luna 5u C8 RP (150 mm x 4,6 mm, 5 μm) column (Phenomenex Inc., Torrance, CA, USA), injection volume: 10 μL , flow rate: 1.5 mL/min at 35 °C; 0 min: 40% MeOH, 60% 0.01M phosphate buffer pH 2.3; 8 min: 85% MeOH, 15% phosphate buffer pH 2.3; 13 min:

85% MeOH, 15% phosphate buffer pH 2.3; 14 min: 40% MeOH, 60% phosphate buffer pH 2.3; 16 min: 40% MeOH, 60% phosphate buffer pH 2.3.

Method B: purity was determined on an Agilent 1100 system (degasser, binary pump, injection module and ColCom setup, Agilent Technologies, Santa Clara, CA, USA) with a Phenomenex Kinetex C8 100A column (150 × 4.6 mm, 2.6 μm) (Phenomenex Inc. Torrance, CA, USA) and detection was performed with a UV DAD at 254 nm and 230 nm wavelength. Elution was carried out with the following gradients: mobile phase A: [H₂O/KH₂PO₄ (solution 0.01 M) (v/v), pH 2.30 (solvent A)], mobile phase B: [MeOH]. 40% B to 95% in 9 min, 95% B for 1 min, 95% B to 40% B in 1 min, 40% B for 5 min, flow rate: 0.5 mL/min.

N-(6-chloro-3-nitropyridin-2-yl)-6-(3,5-dimethoxyphenyl)chinazolin-2-amine (**7A**).

A: 50 mg (0.18 mmol, 1 eq) 6-(3,5-dimethoxyphenyl)quinazolin-2-amine (**12A**), 47 mg (0.20 mmol, 1.1 eq) 2-bromo-6-chloro-3-nitropyridine, 25 mg (0.18 mmol, 1 eq) potassium carbonate, 3 mg (0.02 mmol, 0.1 eq) copper(I) iodide, and 2 mg (0.02 mmol, 0.1 eq) *trans*-1,2-diaminocyclohexane were weighed into a glass tube and dissolved in 2 ml dry 1,4-dioxane. The solution was degassed three times with a membrane pump/ultrasound and purged with argon. The mixture was stirred at 90 °C overnight. The reaction mixture was extracted three times with 5 ml of dichloromethane and then washed twice with 5 ml of demineralized water and once with 5 ml of brine. The combined organic layer was dried with sodium sulfate, concentrated on the rotary evaporator and prepared for further work-up. The mixture was purified by flash column chromatography using the following gradient: PE:EA:DCM 100:0:0 → 0:20:80; 13 CV. The product was obtained as a yellow solid. (7 mg, 9 % yield)

B: 100 mg (0.352 mmol) of 6-(3,5-dimethoxyphenyl)-2-fluoroquinazoline (**15**) were dissolved in 8 ml of dry DMF. 6-Chloro-3-nitropyridin-2-amine (61 mg, 0.352mmol, 1 eq) together with Cs₂CO₃ (172 mg, 0.528 mmol, 1.5 eq) were added sequentially and the reaction mixture was stirred at room temperature for 18 hours. The reaction mixture was diluted with 200 ml of water and extracted with 200 ml of ethyl acetate. The organic layer was washed 3 times with 200 ml of demineralized water and once with 200 ml of brine, dried over sodium sulfate, and evaporated under reduced pressure. The crude product was purified by flash chromatography using the following mobile phase: DCM/EA 50:1 to afford the pure product as a yellow powder (46 mg 30% yield) ¹H NMR

(400 MHz, CDCl₃): δ 10.38 (s, 1H), 9.35 (s, 1H), 8.49 (d, *J* = 8.6 Hz, 1H), 8.12 (d, *J* = 8.8, 1H), 8.04 (s, 1H), 7.97 (d, *J* = 8.8 Hz, 1H), 7.09 (d, *J* = 8.6 Hz, 1H), 6.80 (d, *J* = 2.2 Hz, 2H), 6.53 (t, *J* = 2.2 Hz, 1H), 3.88 (m, 6H). ¹³C NMR (101 MHz, CDCl₃): δ 162.49, 161.51, 155.65, 154.22, 150.53, 147.23, 141.78, 139.47, 137.49, 134.73, 130.91, 127.83, 125.06, 122.76, 117.58, 105.80, 100.07, 55.69. MS (ESI) *m/z* 437.6 [M+H]⁺, HPLC (Method B) *t*_{ret} 9.19 min, purity (254.4 nm) 99.5%, (230.4 nm) 96.0%.

N-(6-chloro-3-nitropyridin-2-yl)-6-(2,6-dichloro-3,5-dimethoxyphenyl)quinazolin-2-amine (**7B**). 70 mg (0.20 mmol, 1 eq) 6-(2,6-dichloro-3,5-dimethoxyphenyl)quinazolin-2-amine (**12B**), 52 mg (0.22 mmol, 1.1 eq) 2-bromo-6-chloro-3-nitropyridine, 28 mg (0.20 mmol, 1 eq) potassium carbonate, 4 mg (0.02 mmol, 0.1 eq) copper(I) iodide, and 2 mg (0.02 mmol, 0.1 eq) *trans*-1,2-diaminocyclohexane were weighed into a glass tube and dissolved in 4 ml dry 1,4-dioxane. The solution was degassed three times with a membrane pump/ultrasound and purged with argon. The mixture was stirred at 90 °C for 7 h. The reaction mixture was extracted three times with 5 ml of ethyl acetate and then washed twice with 5 ml of demineralized water and once with 5 ml of brine. The combined organic layer was dried with sodium sulfate, concentrated on the rotary evaporator, and prepared for further workup. The mixture was separated by flash column chromatograph using the following gradient: PE/EA/DCM 100:0:0 →0:20:80; 16 CV. The product was obtained as a yellow solid. (12 mg, 12% yield) ¹H NMR (400 MHz, DMSO): δ 11.33 (s, 1H), 9.42 (s, 1H), 8.50 (d, *J* = 8.4 Hz, 1H), 7.91 (d, *J* = 1.7 Hz, 1H), 7.70 (dd, *J* = 8.7, 1.9 Hz, 1H), 7.63 (d, *J* = 8.7 Hz, 1H), 7.44 (d, *J* = 8.4 Hz, 1H), 7.03 (s, 1H), 3.98 (s, 6H). ¹³C NMR (101 MHz, DMSO): δ 162.8, 155.3, 154.5, 151.5, 149.3, 145.3, 138.8, 137.9, 136.5, 133.5, 128.7, 125.8, 121.2, 118.8, 112.9, 98.2, 56.8, HRMS (ESI-TOF) *m/z* 506.01913 [M+H]⁺, HPLC (Method A) *t*_{ret} 9.43 min, purity (254.4 nm) 100%, (230.4 nm) 99.3%.

2-chloro-6-(3,5-dimethoxyphenyl)quinazoline (**10A**). 2.27 g (9.33 mmol, 1 eq) 6-bromo-2-chloroquinazoline, 1.70 g (9.33 mmol, 1 eq) (3,5-dimethoxyphenyl)boronic acid, and 5.94 g (28.0 mmol, 3 eq) potassium phosphate were weighed into a 250 ml two-neck flask and dissolved/suspended in 35 ml of dry 1,4-dioxane. The mixture was alternately degassed three times for 30 s using a membrane pump/ultrasound and then purged with argon. Then, 53 mg (0.093 mmol, 0.01 eq) of P(*t*-butyl)₃ Pd G3 as catalyst and 5 ml of demineralized water were added to the batch. The flask was again degassed three times and purged with argon. The mixture was stirred overnight at room

temperature. Under cooling with a mixture of water and ice, about 100 ml of demineralized water was added to the batch, and the product precipitated as brownish flakes. The batch was then stirred under cooling for an additional 5 min. The product was then filtered, washed with water, dried at 50 °C in a hot-air oven to constant weight, and could be used in the subsequent reaction without further purification (2.93 g, 100% yield). ¹H NMR (400 MHz, DMSO): δ 9.62 (s, 1H), 8.55 (d, *J* = 1.2 Hz, 1H), 8.44 (dd, *J* = 9.0, 1.6 Hz, 1H), 8.03 (d, *J* = 8.8 Hz, 1H), 6.97 (d, *J* = 1.7 Hz, 2H), 6.59 (s, 1H), 3.84 (s, 6H). ¹³C NMR (101 MHz, DMSO): δ 164.6, 161.1, 156.5, 150.6, 140.3, 139.8, 135.2, 127.2, 125.5, 123.6, 105.3, 100.4, 55.4. MS (APCI) *m/z* 301.05 [M+H]⁺, HPLC (Method A) *t*_{ret} 8.09 min, purity (254.4 nm) 99.4%, (230.4 nm) 98.3%.

2-chloro-6-(2,6-dichloro-3,5-dimethoxyphenyl)quinazoline (10B). 1.00 g (3.33 mmol, 1 eq) of 2-chloro-6-(3,5-dimethoxyphenyl)quinazoline was weighed into a 250 ml glass flask and dissolved in 50 ml of anhydrous acetonitrile. The mixture was cooled to a temperature between -20 °C to -30 °C with a mixture of acetone and liquid nitrogen. 898 mg (6.61 mmol, 2 eq, 0.534 ml) of sulfuryl chloride was dissolved in 5 ml of anhydrous acetonitrile and added to the reaction mixture at -20 °C. The mixture was stirred at -20 °C for 10 min. Then, 2 ml of demineralized water was added to the reaction. For workup, 100 ml of demineralized water was added to the reaction mixture and stirred for 5 min under cooling with an ice-water mixture. The product which precipitated as brownish flakes was filtered and washed with cold water. The solid was dried in a hot-air oven at 50 °C until constant weight was reached. The product could be used in the subsequent reaction without further purification. (1.24 g, 100% yield) ¹H NMR (400 MHz, DMSO): δ 9.66 (s, 1H), 8.16 (d, *J* = 1.5 Hz, 1H), 8.09 (d, *J* = 8.7 Hz, 1H), 7.95 (dd, *J* = 8.7, 1.8 Hz, 1H), 7.06 (s, 1H), 3.99 (s, *J* = 9.1 Hz, 6H). ¹³C NMR (101 MHz, DMSO): δ 164.6, 157.1, 154.6, 150.6, 138.3, 137.5, 136.9, 128.9, 127.0, 123.2, 112.6, 98.5, 56.8. MS (APCI) *m/z* 368.97 [M+H]⁺, HPLC (Method A) *t*_{ret} 8.70 min, purity (254.4 nm) 96.3%, (230.4 nm) 98.5%.

6-(3,5-dimethoxyphenyl)quinazoline (11A). 250mg (1.195 mmol, 1 eq) of 6-bromoquinazoline was dissolved in a mixture of 15 ml 1,4-dioxane and 2 ml water. Potassium carbonate (0.758 g, 3.58 mmol, 3 eq) and (3,5-dimethoxyphenyl)boronic acid (0.217 g, 1.20 mmol, 1 eq) were added and the reaction mixture was purged with argon. P(*t*-butyl)₃ Pd G3 (6 mg, 0.012 mmol 0.01 eq) was added and the reaction mixture was stirred at room temperature for 18 h. The reaction mixture was

concentrated under reduced pressure, diluted with water (50 ml) and the product was extracted with ethyl acetate (30 ml). The organic layer was dried with sodium sulfate, filtered through a Celite® pad and concentrated under reduced pressure. The crude product was triturated with diethyl ether to obtain pure 6-(3,5-dimethoxyphenyl)quinazoline as yellowish powder (151 mg, 47 % yield) ¹H NMR (400 MHz, CDCl₃): δ 9.46 (s, 1H), 9.34 (s, 1H), 8.27 – 7.96 (m, 3H), 6.82 (d, *J* = 2.2 Hz, 2H), 6.54 (t, *J* = 2.2 Hz, 1H), 3.88 (s, 6H). ¹³C NMR (101 MHz, CDCl₃): δ 161.39, 160.43, 155.19, 149.51, 141.55, 140.92, 134.02, 128.80, 125.26, 124.72, 105.83, 100.06, 55.54. HRMS (ESI-TOF) *m/z* 267.11278 [M+H]⁺, HPLC (Method B) *t*_{ret} 10.29 min, purity (254.4 nm) 99.1%, (230.4 nm) 98.3%.

6-(2,6-dichloro-3,5-dimethoxyphenyl)quinazoline (11B). 150 mg (0.563 mmol, 1 eq) of 6-(3,5-dimethoxyphenyl)quinazoline were dissolved in 10 ml of dry acetonitrile. A solution of sulfonyl chloride (152 mg, 1.13 mmol, 2 eq) in 2 ml of dry acetonitrile was added maintaining the temperature below -20 °C. The mixture was stirred at -20 °C for 1 h. Then, 2 ml of water were added to the cold reaction mixture and left stirring for additional 5 min. The reaction mixture was concentrated under reduced pressure. The crude product was extracted with 10 ml of ethyl acetate. The organic layer was dried with sodium sulfate, evaporated under reduced pressure and purified by flash column chromatography using the following gradient: hexane/EA 100:0 → 50:50; 10 CV. The product was obtained as a beige powder (66 mg 35% yield) ¹H NMR (400 MHz, DMSO): δ 9.66 (s, 1H), 9.36 (s, 1H), 8.17 – 8.04 (m, *J* = 18.2, 5.0 Hz, 2H), 7.87 (dd, *J* = 8.7, 1.7 Hz, 1H), 7.05 (s, 1H), 3.98 (s, 6H). ¹³C NMR (101 MHz, DMSO): δ 160.90, 155.62, 154.61, 148.77, 138.75, 136.48, 136.01, 128.45, 127.94, 124.56, 112.75, 98.38, 56.84. HRMS (ESI-TOF) *m/z* 335.03498 [M+H]⁺, HPLC (Method B) *t*_{ret} 10.91 min, purity (254.4 nm) 98.0%, (230.4 nm) 99.1%.

6-(3,5-dimethoxyphenyl)quinazolin-2-amine (12A). 300 mg (0.998 mmol, 1 eq) of 2-chloro-6-(3,5-dimethoxyphenyl)quinazoline was weighed into a microwave tube and dissolved in 6 ml of 1,4-dioxane. To the tube 1 ml of aqueous ammonia solution (25%) was added and a white solid precipitated. The mixture was stirred in a microwave oven at 75 °C for 2 h. To the solution, 10 ml of demineralized water were added under cooling with an ice-water mixture and the product precipitated as a white solid, which was filtered off, washed with water, and dried in a hot-air oven at 50 °C to constant weight. The product could be used in the subsequent reaction without further purification.

(308 mg, 100% yield) ^1H NMR (400 MHz, DMSO): δ 9.17 (s, 1H), 8.13 (d, J = 2.0 Hz, 1H), 8.03 (dd, J = 8.8, 2.1 Hz, 1H), 7.48 (d, J = 8.8 Hz, 1H), 6.92 (s, 2H), 6.88 (d, J = 2.2 Hz, 2H), 6.51 (t, J = 2.1 Hz, 1H), 3.83 (s, 6H). ^{13}C NMR (101 MHz, DMSO): δ 163.2, 161.4, 161.4, 151.9, 142.0, 133.9, 133.6, 125.9, 125.4, 120.0, 105.1, 99.7, 55.8. MS (ESI) m/z 350.2 $[\text{M}+\text{H}]^+$, HPLC (Method A) t_{ret} 4.69 min, purity (254.4 nm) 98.2%, (230.4 nm) 96.3%.

6-(2,6-dichloro-3,5-dimethoxyphenyl)quinazolin-2-amine (12B). 500 mg (1.35 mmol, 1 eq) of 2-chloro-6-(2,6-dichloro-3,5-dimethoxyphenyl)quinazoline was weighed into a microwave tube and dissolved in 4 ml of 1,4-dioxane. 1 ml of aqueous ammonia solution (25%) was added to the tube. The mixture was stirred in a microwave oven at 75 °C for 2 h and the product precipitated partially as a white solid. The suspension was mixed with 10 ml of demineralized water under cooling with an ice-water mixture to further precipitate the product. The product was then filtered and washed with cold water. The solid was dried in a hot-air oven at 50 °C until constant weight was reached and could be used in the subsequent reaction without further purification. (442 mg, 93% yield) ^1H NMR (400 MHz, DMSO): δ 9.14 (s, 1H), 7.65 (s, 1H), 7.49 (s, 2H), 7.00 (s, 1H), 6.97 (s, 2H), 3.97 (s, 6H). ^{13}C NMR (101 MHz, DMSO): δ 163.0, 161.7, 154.9, 151.8, 139.9, 135.8, 130.7, 128.9, 124.9, 119.6, 113.6, 98.4, 57.2. MS (ESI) m/z 282.2 $[\text{M}+\text{H}]^+$, HPLC (Method A) t_{ret} 4.26 min, purity (254.4 nm) 98.9%, (230.4 nm) 97.4%.

6-(3,5-dimethoxyphenyl)-N-(3-nitropyridin-2-yl)quinazolin-2-amine (13A). 100 mg (0.355 mmol) of 6-(3,5-dimethoxyphenyl)quinazolin-2-amine were dissolved in 20 ml of dry 1,4-dioxane. 2-bromo-3-nitropyridine (72 mg 0.355 mmol, 1 eq) and cesium carbonate (173.5 mg, 0.53 mmol, 1.5eq) were added to the reaction mixture, followed by $\text{Pd}_2(\text{dba})_3$ (16 mg 0.018 mmol, 0.05 eq) and XantPhos (11 mg 0.018 mmol, 0.05 eq). The reaction mixture was purged with argon and stirred at 100 °C for 18 h. The reaction mixture was then concentrated under reduced pressure. 20 ml of water were added and the product was extracted with 20 ml of ethyl acetate. The organic layer was dried with sodium sulfate and evaporated under reduced pressure. The crude product was purified by flash column chromatography using the following gradient: hexane/EA 100:0 \rightarrow 50:50; 10 CV. The product was obtained as a yellow powder (43 mg, 30% yield) ^1H NMR (400 MHz, CDCl_3): δ 10.31 (s, 1H), 9.35 (s, 1H), 8.73 (dd, J = 4.5, 1.6 Hz, 1H), 8.56 (dd, J = 8.3, 1.7 Hz, 1H), 8.09 (dd, J = 8.8, 2.1 Hz, 1H), 8.02 (d, J = 1.8 Hz, 1H), 7.95 (d, J = 8.8 Hz, 1H), 7.13 (dd, J = 8.3, 4.6 Hz, 1H), 6.81 (d, J = 2.2 Hz,

2H), 6.52 (t, $J = 2.2$ Hz, 1H), 3.88 (s, 6H). ^{13}C NMR (101 MHz, CDCl_3): δ 162.50, 161.49, 154.92, 154.50, 150.76, 147.46, 141.83, 139.03, 135.24, 134.56, 132.66, 127.77, 125.06, 122.50, 117.33, 105.73, 100.03, 55.68. MS (ESI) m/z 403.9 $[\text{M}+\text{H}]^+$, HPLC (Method B) t_{ret} 11.82 min, purity (254.4 nm) 98.6%, (230.4 nm) 97.8%.

6-(2,6-dichloro-3,5-dimethoxyphenyl)-N-(3-nitropyridin-2-yl)quinazolin-2-amine (13B). 100 mg (0.29 mmol, 1 eq) 6-(2,6-dichloro-3,5-dimethoxyphenyl)quinazolin-2-amine, 64 mg (0.31 mmol, 1.1 eq) 2-bromo-3-nitropyridine, 40 mg (0.29 mmol, 1 eq) potassium carbonate, 5 mg (0.03 mmol, 0.1 eq) copper(I) iodide, and 3 mg (0.03 mmol, 0.1 eq) *trans*-1,2-diaminocyclohexane were weighed into a glass tube and dissolved in 2 ml of dry 1,4-dioxane. The solution was degassed three times with a membrane pump/ultrasonic and purged with argon. The mixture was stirred at 90 °C overnight. The reaction mixture was extracted three times with 5 ml of dichloromethane and then washed twice with 5 ml of demineralized water and once with 5 ml of brine. The combined organic layer was dried with sodium sulfate, concentrated on the rotary evaporator, and the crude product was purified by flash column chromatography, using the following gradient: PE/EA 100:0 \rightarrow 30:70; 10 CV. The product was obtained as a yellow solid. (17 mg, 13% yield) ^1H NMR (400 MHz, DMSO): δ 11.03 (s, 1H), 9.39 (s, 1H), 8.67 (dd, $J = 4.7, 1.6$ Hz, 1H), 8.45 (dd, $J = 8.1, 1.6$ Hz, 1H), 7.88 (d, $J = 1.7$ Hz, 1H), 7.67 (dd, $J = 8.7, 1.9$ Hz, 1H), 7.59 (d, $J = 8.7$ Hz, 1H), 7.38 (dd, $J = 8.1, 4.7$ Hz, 1H), 7.03 (s, 1H), 3.98 (s, 6H). ^{13}C NMR (101 MHz, DMSO): δ 162.7, 155.8, 154.5, 152.3, 149.5, 145.0, 138.9, 137.9, 136.3, 134.4, 133.0, 128.7, 125.6, 121.0, 119.2, 112.9, 98.2, 56.8. HRMS (ESI-TOF) m/z 472.05826 $[\text{M}+\text{H}]^+$, HPLC (Method A) t_{ret} 8.81 min, purity (254.4 nm) 99.0%, (230.4 nm) 98.2%.

6-(3,5-dimethoxyphenyl)-N-(6-methyl-3-nitropyridin-2-yl)quinazolin-2-amine (14). 100 mg (0.355 mmol) of 6-(3,5-dimethoxyphenyl)quinazolin-2-amine were dissolved in 20 ml of dry 1,4-dioxane. 2-bromo-6-methyl-3-nitropyridine (76 mg, 0.355 mmol, 1 eq) and cesium carbonate (173.5 mg, 0.53 mmol, 1.5 eq) were added to the reaction mixture, followed by $\text{Pd}_2(\text{dba})_3$ (16 mg 0.018 mmol, 0.05 eq) and Xantphos (11 mg, 0.018 mmol, 0.05 eq). The reaction mixture was purged with argon and stirred at 100 °C for 18h. The reaction mixture was concentrated under reduced pressure. 20 ml of water were added and the product was extracted with 20 ml of ethyl acetate. The organic layer was dried with sodium sulfate and evaporated under reduced pressure. The crude product was purified by preparative thin layer chromatography using the

following mobile phase: EA/MeOH (95:5). The product was obtained as a yellow powder (26 mg, 18% yield) ^1H NMR (400 MHz, CDCl_3): δ 10.17 (s, 1H), 9.31 (s, 1H), 8.41 (d, $J = 8.4$ Hz, 1H), 8.07 (d, $J = 8.8$, 1H), 8.00 (d, $J = 1.5$ Hz, 1H), 7.91 (d, $J = 8.8$ Hz, 1H), 6.96 (d, $J = 9.1$ Hz, 1H), 6.80 (d, $J = 2.1$ Hz, 2H), 6.52 (s 1H), 3.88 (s, 6H), 2.63 (s, 3H). ^{13}C NMR (101 MHz, CDCl_3): δ 165.08, 162.17, 161.35, 154.85, 150.64, 146.71, 141.79, 138.73, 135.10, 134.29, 130.74, 127.59, 124.92, 122.33, 117.34, 105.60, 99.84, 55.54, 25.13. HRMS (ESI-TOF) m/z 418.15144 $[\text{M}+\text{H}]^+$, HPLC (Method B) t_{ret} 11.99 min, purity (254.4 nm), 98.8%, (230.4 nm) 97.0%.

6-(3,5-dimethoxyphenyl)-2-fluoroquinazoline (15). 181 mg (0.998 mmol, 1.5 eq) of $\text{Me}_4\text{NF}\cdot t\text{-AmylOH}$ (synthesized by the procedure of Morales-Colón et al. [57]) were dissolved in 10 ml of dry DMSO. 200 mg (0.665 mmol) of 2-chloro-6-(3,5-dimethoxyphenyl)quinazoline were added and the reaction mixture was stirred at room temperature for 18h. The reaction mixture was diluted with water (50 ml) extracted with ethyl acetate (50 ml) and the organic layer was washed three times with 50 ml of demineralized water and once with 50 ml of brine. The organic layer was dried with sodium sulfate and evaporated under reduced pressure. The crude product was purified by column chromatography using Hex/EA (3:1) as the eluent. The purified product contains about 10% of the starting material and was obtained as a yellowish powder (102 mg, 54% yield). ^1H NMR (400 MHz, CDCl_3): δ 9.40 (d, $J = 2.1$ Hz, 1H), 8.18 (dd, $J = 8.8, 1.8$ Hz, 1H), 8.13 (d, $J = 1.7$ Hz, 1H), 8.02 (d, $J = 8.8$ Hz, 1H), 6.79 (d, $J = 2.2$ Hz, 2H), 6.54 (t, $J = 2.2$ Hz, 1H), 3.88 (s, 6H). ^{13}C NMR (101 MHz, CDCl_3): δ 165.61 (d, $J = 14.1$ Hz), 161.57, 160.32 (d, $J = 219.1$ Hz), 151.82 (d, $J = 13.1$ Hz), 141.34, 140.57 (d, $J = 2.5$ Hz), 135.57, 127.99 (d, $J = 2.7$ Hz), 125.00, 124.15 (d, $J = 3.2$ Hz), 105.92, 100.21, 55.68. HPLC (Method B) t_{ret} 8.12 min, purity (254.4 nm) 89.6%, (230.4 nm) 90.1%.

2-bromo-6-(3,5-dimethoxyphenyl)quinazolin (16). 1.00 g (3.33 mmol, 1 eq) 2-chloro-6-(3,5-dimethoxyphenyl)quinazoline was dissolved in 40 ml of propionitrile and 1.53 g (9.98 mmol, 3 eq) of bromotrimethylsilane were added, which resulted in the precipitation of a yellow solid. The mixture was refluxed overnight and then poured into 40 ml of 2 M aqueous sodium hydroxide solution containing about 40 g of ice. The aqueous layer was extracted three times with 40 ml of ethyl acetate and the combined organic layer washed twice with 40 ml of demineralized water and once with 40 ml of brine. The organic layer was dried with sodium sulfate, then concentrated to dryness

on a rotary evaporator and purified by flash column chromatography, using the following gradient: PE/EA/DCM 100:0:0 → 0:5:95; 11 CV. The product was obtained as a beige solid. (351 mg, 31% yield) ^1H NMR (400 MHz, DMSO): δ 9.54 (s, 1H), 8.53 (d, J = 1.6 Hz, 1H), 8.43 (dd, J = 8.8, 1.9 Hz, 1H), 8.03 (d, J = 8.8 Hz, 1H), 6.98 (d, J = 2.0 Hz, 2H), 6.61 – 6.58 (m, 1H), 3.84 (s, 6H). ^{13}C NMR (101 MHz, DMSO): δ 164.0, 161.1, 150.8, 148.4, 140.3, 139.9, 135.1, 127.2, 125.6, 123.8, 105.3, 100.4, 55.4. HPLC (Method A) t_{ret} 8.66 min, purity (254.4 nm) 97.4%, (230.4 nm) 96.4%.

2-chloro-8-(4,4,5,5-tetramethyl-1,3,2-dioxaborolan-2-yl)quinazolin (17): 400 mg (1.64 mmol, 1 eq) of 8-bromo-2-chloroquinazoline, 417 mg (1.64 mmol, 1 eq) of 4,4,4',4',5,5,5',5'-octamethyl-2,2'-bi(1,3,2-dioxaborolane) and 484 mg (4.93 mmol, 3 eq) of potassium acetate were weighed into a 50 ml two-neck flask and dissolved in 10 ml of 1,4-dioxane. The flask was degassed three times with a membrane pump and then purged with argon. To the solution 60 mg (0.08 mmol, 0.05 eq) Pd(dppf)Cl₂ was added and it was again degassed three times and purged with argon. The batch was stirred for 4 h at 95 °C. The mixture was taken up in 20 ml ethyl acetate and washed twice with 20 ml of demineralized water and once with 20 ml of brine. The combined organic layer was dried with sodium sulfate, then concentrated on the rotary evaporator, and the resulting solid could be used in the subsequent reaction without further purification. ^1H NMR (400 MHz, DMSO): δ 9.59 (s, 1H), 8.31 – 8.24 (m, 2H), 7.79 (t, J = 7.5 Hz, 1H), 1.36 (s, 12H). ^{13}C NMR (101 MHz, DMSO) δ 164.61, 156.44, 153.94, 142.11, 130.49, 127.95, 122.90, 84.02, 81.34, 73.50, 24.62. MS (ESI) m/z 213.1 [M+H]⁺, HPLC (Method A) t_{ret} 6.24 min, purity (254.4 nm) 92.4%, (230.4 nm) 97.0%.

2'-Chloro-6-(3,5-dimethoxyphenyl)-2,8'-biquinazoline (18). 50 mg (0.15 mmol, 1 eq) 2-bromo-6-(3,5-dimethoxyphenyl)quinazoline, 51 mg (0.17 mmol, 1.2 eq) 2-chloro-8-(4,4,5,5-tetramethyl-1,3,2-dioxaborolan-2-yl)quinazoline and 92 mg (0.44 mmol, 3 eq) potassium phosphate were weighed into a glass tube and dissolved in 4 ml of 1,4-dioxane. The solution was degassed three times with a membrane pump/ultrasound and purged with argon. To the solution 8 mg (0.015 mmol, 0.1 eq) of P(*t*-butyl)₃ Pd G3 pre-catalyst and 1 ml of demineralized water were added, and it was again degassed three times and purged with argon. The mixture was stirred at room temperature overnight. The solution was extracted three times with 5 ml of ethyl acetate and then washed twice with 5 ml of water and once with 5 ml of brine. The combined organic

layer was dried with sodium sulfate, then concentrated on the rotary evaporator and prepared for further workup. The mixture was purified by flash column chromatography, using the following gradient: PE/EA/DCM 100:0:0 → 0:5:95; 11 CV. The product was obtained as a yellow solid (18 mg, 36% yield). ¹H NMR (400 MHz, DMSO): δ 9.60 – 9.55 (m, *J* = 4.3 Hz, 1H), 9.37 – 9.31 (m, *J* = 4.1 Hz, 1H), 8.40 – 8.34 (m, *J* = 7.1 Hz, 1H), 8.20 – 8.07 (m, *J* = 17.1, 11.0, 6.6 Hz, 4H), 7.84 – 7.76 (m, 1H), 6.82 – 6.76 (m, *J* = 2.1 Hz, 2H), 6.52 – 6.46 (m, 1H), 3.86 – 3.80 (m, *J* = 4.0 Hz, 6H). ¹³C NMR (101 MHz, DMSO): δ 163.3, 161.4, 160.6, 157.9, 149.9, 141.5, 141.4, 137.4, 136.9, 134.6, 129.3, 128.7, 128.1, 124.8, 123.8, 123.7, 105.9, 100.2, 55.5. HRMS (ESI-TOF) *m/z* 429.11152 [M+H]⁺, HPLC (Method A) *t*_{ret} 8.40 min, purity (254.4 nm) 97.6%, (230.4 nm) 97.1%.

2-(2-chloro-7H-pyrrolo[2,3-d]pyrimidin-7-yl)-6-(3,5-dimethoxyphenyl)quinazolin (**19**). 30 mg (0.09 mmol, 1 eq) of 2-bromo-6-(3,5-dimethoxyphenyl)quinazoline, 17 mg (0.11 mmol, 1.3 eq) of 2-chloro-7H-pyrrolo[2,3-d]pyrimidine, 37 mg (0.17 mmol, 2 eq) of potassium phosphate, 2 mg (0.01 mmol, 0.1 eq) of copper(I) iodide, and 1 mg (0.01 mmol, 0.1 eq) of *trans*-1,2-diaminocyclohexane were weighed into a glass tube and dissolved/suspended in 2 ml 1,4-dioxane. The mixture was degassed three times with a membrane pump/ultrasound, purged with argon and stirred for 4 h at 100 °C. The reaction mixture was extracted three times with 5 ml of ethyl acetate and the combined organic layers were washed twice with 5 ml of demineralized water and once with 5 ml of brine. The organic layer was dried with sodium sulfate, concentrated on the rotary evaporator and the crude product purified by flash column chromatography using the following gradient: EA/DCM 0:100 → 10:90; 9 CV The product was obtained as a white solid (10 mg, 57% yield). ¹H NMR (400 MHz, DMSO): δ 9.86 (s, 1H), 9.12 (s, 1H), 8.61 (d, *J* = 2.0 Hz, 1H), 8.48 (dd, *J* = 7.4, 3.5 Hz, 2H), 8.13 (d, *J* = 8.8 Hz, 1H), 7.07 – 7.00 (m, *J* = 7.2, 3.0 Hz, 3H), 6.62 (t, *J* = 2.1 Hz, 1H), 3.90 – 3.85 (m, *J* = 10.5 Hz, 6H). ¹³C NMR (101 MHz, DMSO): δ 163.8, 161.1, 153.8, 152.4, 151.9, 151.7, 149.7, 140.5, 139.0, 135.0, 129.9, 127.7, 125.6, 123.4, 120.1, 105.2, 103.1, 100.4, 55.5. HRMS (ESI-TOF) *m/z* 440.08898 [M+H]⁺, HPLC (Method A) *t*_{ret} 9.31 min, purity (254.4 nm) 96.6%, (230.4 nm) 95.9%.

6-(3,5-dimethoxyphenyl)quinazolin-2-thiol (**20**). 500 mg (1.66 mmol, 1 eq) of 2-chloro-6-(3,5-dimethoxyphenyl)quinazoline and 266 mg (3.33 mmol, 2 eq) of thiourea were dissolved in 4 ml of ethanol and refluxed for 6 h which resulted in the precipitation of a

yellow solid. The reaction mixture was cooled with ice water, the precipitate was collected by filtration and washed with 15 ml of ethanol. The filter cake was suspended in 10 ml of ethanol without further workup, to which one equivalent of 0.1 M sodium hydroxide solution was added, and stirred at room temperature for 1 h. The mixture was cooled with ice water and 20 ml of demineralized water were added, precipitating a yellow solid. The solid was then filtered, washed with cold water, dried in hot-air oven, and could be used in the subsequent reactions without further purification (240 mg, 48% yield). ¹H NMR (400 MHz, DMSO): δ 7.65 – 7.60 (m, 2H), 7.12 (d, *J* = 9.1 Hz, 1H), 6.73 (d, *J* = 2.2 Hz, 2H), 6.44 (t, *J* = 2.1 Hz, 1H), 5.56 (s, 1H), 4.12 (s, 6H). ¹³C NMR (101 MHz, DMSO): δ 175.2, 161.7, 142.2, 135.9, 135.3, 128.7, 126.5, 118.8, 115.2, 105.0, 99.6, 80.5, 55.5. MS (ESI) *m/z* 321.1 [M+H]⁺, HPLC (Method A) *t*_{ret} 6.64 min, purity (254.4 nm) 99.4%, (230.4 nm) 99.0%.

2-((6-chloro-3-nitropyridin-2-yl)thio)-6-(3,5-dimethoxyphenyl)quinazolin (21). 25 mg (0.08 mmol, 1 eq) of 6-(3,5-dimethoxyphenyl)quinazoline-2-thiol and 10 mg (0.09 mmol, 1.1 eq) of potassium *tert*-butoxide were weighed into a glass tube and dissolved in 2 ml of dry tetrahydrofuran. The mixture was stirred for 30 min under cooling with an ice-water mixture at 0 °C. Subsequently, 18 mg (0.10 mmol, 1.2 eq) of 6-chloro-2-fluoro-3-nitropyridine were added to the batch and stirred again for 2 h at 0 °C. The reaction mixture became a clear yellow solution. The reaction solution was then mixed with 10 ml of ethyl acetate, washed twice with 5 ml of demineralized water and once with 5 ml of brine. The organic layer was then dried with sodium sulfate and prepared on the rotary evaporator for further workup. The mixture was purified by flash column chromatography, using the following gradient: PE/EA 100:0 → 30:70; 18 CV The product was obtained as a yellow solid (22 mg, 57% yield). ¹H NMR (400 MHz, DMSO): δ 9.65 (s, 1H), 8.77 (dd, *J* = 5.3, 1.9 Hz, 1H), 8.56 (d, *J* = 1.6 Hz, 1H), 8.45 (dd, *J* = 8.8, 1.9 Hz, 1H), 8.35 – 8.31 (m, 1H), 8.06 (d, *J* = 8.8 Hz, 1H), 7.01 (d, *J* = 2.1 Hz, 2H), 6.63 – 6.60 (m, 1H), 3.86 (s, 6H). ¹³C NMR (101 MHz, DMSO): δ 162.4, 162.0, 161.1, 153.0, 152.9, 149.6, 143.6, 140.4, 140.0, 137.4, 134.7, 127.5, 125.6, 123.4, 123.3, 105.3, 100.4, 55.4. HRMS (ESI-TOF) *m/z* 455.05838 [M+H]⁺, HPLC (Method A) *t*_{ret} 9.31min, purity (254.4 nm) 96.8%, (230.4 nm) 96.4%.

2-((2-chloropyrimidin-4-yl)thio)-6-(3,5-dimethoxyphenyl)quinazolin (22). 40 mg (0.13 mmol, 1 eq) 6-(3,5-dimethoxyphenyl)quinazoline-2-thiol and 17 mg (0.15 mmol, 1.1 eq) potassium *tert*-butoxide were weighed into a glass tube, dissolved in 3 ml of

dry tetrahydrofuran, and stirred at room temperature for 30 min. To the mixture 24 mg (0.16 mmol, 1.2 eq) of 2,4-dichloropyrimidine was added and stirred for another 2 h. The reaction mixture became a clear yellow solution. The reaction solution was then mixed with 10 ml dichloromethane, washed twice with 5 ml demineralized water and once with 5 ml brine. The combined organic layer was then dried with sodium sulfate and prepared on the rotary evaporator for further workup. The mixture was purified by flash column chromatography, using the following gradient: PE:EA 100:0 → 20:80; 18 CV The product was obtained as a yellow solid (29 mg, 53% yield). ¹H NMR (400 MHz, DMSO): δ 9.64 (s, 1H), 8.75 (d, *J* = 4.8 Hz, 1H), 8.55 (s, 1H), 8.45 (d, *J* = 8.3 Hz, 1H), 8.37 (d, *J* = 5.3 Hz, 1H), 8.05 (d, *J* = 8.7 Hz, 1H), 7.07 – 6.94 (m, *J* = 22.2 Hz, 2H), 6.61 (s, 1H), 3.85 (s, 6H). ¹³C NMR (101 MHz, DMSO): δ 169.8, 162.6, 161.8, 161.1, 159.9, 159.2, 149.5, 140.4, 139.7, 134.9, 127.3, 125.7, 123.5, 120.9, 105.3, 100.4, 55.5. HRMS (ESI-TOF) *m/z* 433.05040 [M+H]⁺, HPLC (Method A) *t*_{ret} 9.39 min, purity (254.4 nm) 99.6%, (230.4 nm) 97.8%.

6-(3,5-dimethoxyphenyl)-2-((2-fluoropyrimidin-4-yl)thio)quinazolin (**23**). 40 mg (0.13 mmol, 1 eq) 6-(3,5-dimethoxyphenyl)quinazoline-2-thiol and 17 mg (0.15 mmol, 1.1 eq) potassium tert-butoxide were weighed into a glass tube, dissolved in 3 ml of dry tetrahydrofuran, and stirred at room temperature for 30 min. To the mixture 19 mg (0.16 mmol, 1.2 eq) of 2,4-difluoropyrimidine was added and stirred again at room temperature for another 2 h. The reaction mixture became a clear yellow solution. The batch was then mixed with 10 ml of demineralized water under cooling with an ice-water mixture where the product precipitated as a white solid. The suspension was then filtered off and washed with water. The residue was dried in a hot-air oven until a constant weight is reached and could be used without further purification (42 mg, 79% yield). ¹H NMR (400 MHz, DMSO): δ 9.65 (s, 1H), 8.78 (dd, *J* = 5.3, 1.9 Hz, 1H), 8.56 (d, *J* = 1.7 Hz, 1H), 8.45 (dd, *J* = 8.8, 2.0 Hz, 1H), 8.36 – 8.30 (m, 1H), 8.07 (d, *J* = 8.8 Hz, 1H), 7.01 (d, *J* = 2.1 Hz, 2H), 6.61 (t, *J* = 1.9 Hz, 1H), 3.85 (s, 6H). ¹³C NMR (101 MHz, DMSO): δ 171.1, 170.1, 162.6, 162.3, 161.6, 161.2, 161.1, 161.1, 160.1, 149.6, 140.4, 139.7, 134.9, 127.4, 125.7, 123.5, 120.2, 120.1, 105.3, 100.4, 55.5. HRMS (ESI-TOF) *m/z* 417.07998 [M+H]⁺, HPLC (Method A) *t*_{ret} 9.06 min, purity (254.4 nm), 96.3% (230.4 nm) 96.2%.

2-((2-chloro-5-fluoropyrimidin-4-yl)thio)-6-(3,5-dimethoxyphenyl)quinazolin (**24**). 40 mg (0.13 mmol, 1 eq) of 6-(3,5-dimethoxyphenyl)quinazoline-2-thiol and 17 mg

(0.15 mmol, 1.1 eq) of potassium *tert*-butoxide were weighed into a glass tube, dissolved/suspended in 3 ml of dry tetrahydrofuran, and stirred at room temperature for 30 min. To the batch 27 mg (0.16 mmol, 1.2 eq) of 2,4-dichloro-5-fluoropyrimidine were added and the mixture stirred again at room temperature for another 2 h. The reaction mixture was then mixed with 10 ml of dichloromethane, washed twice with 5 ml of demineralized water and once with 5 ml of brine. The organic layer was dried with sodium sulfate, concentrated on the rotary evaporator, and the mixture was purified by flash column chromatography, using the following gradient: PE/EA 100:0 → 30:70; 15 CV The product was obtained as a white solid (36 mg, 63% yield). ¹H NMR (400 MHz, DMSO): δ 9.57 (s, 1H), 9.01 (d, *J* = 1.0 Hz, 1H), 8.49 (d, *J* = 1.8 Hz, 1H), 8.39 (dd, *J* = 8.9, 2.1 Hz, 1H), 7.92 (d, *J* = 8.8 Hz, 1H), 6.97 (d, *J* = 2.2 Hz, 2H), 6.59 (t, *J* = 2.1 Hz, 1H), 3.84 (s, 6H). ¹³C NMR (101 MHz, DMSO): δ 162.7, 161.7, 161.1, 156.8 (d, *J* = 263.5 Hz), 154.5 (d, *J* = 18.1 Hz), 153.7 (d, *J* = 3.9 Hz), 149.6, 148.1 (d, *J* = 25.5 Hz), 140.4, 139.6, 135.0, 127.1, 125.7, 123.1, 105.3, 100.3, 55.4. HRMS (ESI-TOF) *m/z* 451.04065 [M+H]⁺, HPLC (Method A) *t*_{ret} 9.53 min, purity (254.4 nm) 100%, (230.4 nm) 99.4%.

6-(3,5-dimethoxyphenyl)-2-((3-nitropyridin-2-yl)thio)quinazolin (**25**). 40 mg (0.13 mmol, 1 eq) of 6-(3,5-dimethoxyphenyl)quinazoline-2-thiol and 17 mg (0.15 mmol, 1.1 eq) of potassium *tert*-butoxide were weighed into a glass tube, dissolved in 2 ml dry tetrahydrofuran, and stirred at room temperature for 30 min. To the reaction mixture 23 mg (0.16 mmol, 1.2 eq) of 2-fluoro-3-nitropyridine were added and stirred again at room temperature for another 2 h. The batch was then mixed with 10 ml of dichloromethane, washed twice with 5 ml of demineralized water and once with 5 ml of brine. The organic layer was dried with sodium sulfate, concentrated on the rotary evaporator, and the crude product mixture was purified by flash column chromatography using the following gradient: PE/EA 100:0 → 30:70; 10 CV. The product was obtained as a yellow solid (11 mg, 20% yield). ¹H NMR (400 MHz, DMSO): δ 9.57 (d, *J* = 0.6 Hz, 1H), 8.74 (dd, *J* = 4.6, 1.6 Hz, 1H), 8.65 (dd, *J* = 8.3, 1.6 Hz, 1H), 8.50 (d, *J* = 1.9 Hz, 1H), 8.39 (dd, *J* = 8.8, 2.1 Hz, 1H), 7.94 (d, *J* = 8.8 Hz, 1H), 7.66 (dd, *J* = 8.3, 4.6 Hz, 1H), 6.99 (d, *J* = 2.2 Hz, 2H), 6.60 (t, *J* = 2.2 Hz, 1H), 3.85 (s, 6H). ¹³C NMR (101 MHz, DMSO): δ 163.0, 162.3, 161.1, 153.6, 151.0, 149.5, 145.2, 140.5, 139.6, 134.6, 134.2, 127.3, 125.5, 123.3, 123.2, 105.3, 100.3, 55.4. HRMS (ESI-TOF) *m/z* 421.09729 [M+H]⁺, HPLC (Method A) *t*_{ret} 8.70 min, purity (254.4 nm) 95.1%, (230.4 nm) 95.8%.

Molecular Modelling. Molecular modeling was performed using the Schrödinger Small-Molecule Drug Discovery Suite 2020-3 (Schrödinger, LLC, New York, NY, USA). Proteins-ligand complexes used for docking were prepared using the standard protein preparation protocol implemented in the Schrödinger Software package (protein preparation wizard). Briefly, bond orders were automatically assigned, C- and N-termini capped, missing side chains inserted and the structures refined using the Prime module. PROPKA was used for assigning protonation states at physiological pH and hydrogen bond orientations/tautomers were optimized during protein preparation. Waters molecules were deleted and all structures manually checked prior to docking. For covalent docking, the CovDock module was applied in the pose prediction mode using standard settings and a minimization radius set to 3Å. Three poses were predicted for each ligand and the highest ranked pose was selected. The figures were generated with PyMOL 2.5.4. (Schrödinger, LLC, New York, NY, USA).

Biochemical Assays. The provided IC₅₀ values were measured using the HotSpot™ Kinase Profiling assay conducted at Reaction Biology Corp. in their facilities in Malvern, PA, USA. All IC₅₀ values were first determined by singlicate measurements starting at a concentration of 5 μM with a 10-fold serial dilution (5-point measurement). Duplicate re-determinations for FGFR4 were performed for the most active compounds **7A** and **7B**. The IC₅₀ values for the compounds **7A**, **7B**, and the reference **BLU9931** were additionally determined with the PhosphoSens® CSox-based continuous assay format at AssayQuant Technologies, Inc. Here, the compounds were prepared through serial dilution in 100% DMSO, starting at 0.1 μM and diluting 3-fold. IC₅₀ values were determined using the first 20 minutes of the steady-state linear range of the assay. Final reaction conditions: 50 mM HEPES, pH 7.5, ATP concentration at *K_m*, 1.0 mM DTT, 0.01% Brij-35, 0.5 mM EGTA, 1% glycerol, 10 mM MgCl₂, 0.20 mg/mL BSA, 15 μM AQT sensor substrate (AQT0101), 2% DMSO. FGFR4 cytoplasmic domain (460-802), N-terminal GST fusion, Carna (cat. # 08-136/ Lot: 17CBS-0513 M). Reaction setup (0 min; all steps before readout performed at room temp.): 11.7 μL reaction mix (HEPES, Brij, EGTA, MgCl₂), DTT, ATP & CSox substrate, 0.3 μL inhibitor dilution in 100% DMSO, 3.0 μL enzyme dilution buffer (EDB) or kinase (5x in EDB). 15 μL final reaction volume. The reaction was run at 30°C for 240 minutes. The reactions were

run in PerkinElmer 384-well low volume white ProxiPlates (Cat. #6059480) after sealing using optically-clear adhesive film (TopSealA-Plus plate seal, PerkinElmer [Cat. #6050185]) in a Biotek Synergy Neo 2 microplate reader with excitation (360 nm) and emission (485 nm) wavelengths. IC₅₀ values were determined starting at a concentration of 0.1 μM with a 3-fold serial dilution (20-point measurement).

Cellular viability study. Hep3B cells were purchased from the American Type Culture Collection. The cells were cultured in DMEM medium supplemented with 10% FBS at 37°C and 7.5% CO₂. Mycoplasma contamination was excluded via a PCR-based method. The cells were treated with the compounds at indicated concentrations starting at 10 μM with a 3-fold serial dilution (10-point measurement) for 4 days. The cell viability was evaluated by CellTiter-Glo (CTG) based luminescent assay (Promega). The data were analyzed using GraphPad Prism (v9.4.1) software. Experiments were run in triplicate and three biological replicates were performed each yielding similar results.

Determination of kinetic constants. The k_{inact}/K_i values for the compounds **7A** and **7B** and **BLU9931** were determined with a PhosphoSens® CSox-based continuous assay format at AssayQuant Technologies, Inc. All inhibitors in this set were able to be fit to a two-step global model, allowing for independent k_{inact} and K_i determination. Reaction Conditions: 50 mM HEPES, pH 7.5, ATP concentration at K_m , 1.0 mM DTT, 0.01% Brij-35, 0.5 mM EGTA, 1% glycerol (from EDB), 10 mM MgCl₂, 0.2 mg/mL BSA (from EDB), 15 μM AQT sensor substrate (AQT0101), 1% DMSO. FGFR4, cytoplasmic domain (460-802), N-terminal GST fusion, Carna (cat. # 08-136/ Lot: 17CBS-0513 M). Reaction setup: 0.3 μL compound dilution, 3.0 μL 10X Sox-based Substrate, 3.0 μL 10X ATP, 30 minute incubation at RT (while reaction mix is made), 23.7 μL reaction mix with 1.4X enzyme or EDB and all other components (enzyme/EDB added just before use of reaction mix), 30 μL final reaction volume. The reaction was run at 30°C for 120 minutes. It was performed with a 1.5 serial dilution (24 point measurement) starting with a concentration of 0.05 μM.

Metabolic stability. Pooled liver microsomes from humans (male) were purchased from *Sekisui XenoTech, LLC*, Kansas City, KS, USA. Metabolic stability assays were performed in the presence of an NADPH-regenerating system consisting of 5 mM glucose-6-phosphate, 5 U/mL glucose-6-phosphate dehydrogenase, and 1 mM NADP⁺. Liver microsomes (20 mg/mL), the NADPH-regenerating system, and 4 mM of

MgCl₂·6 H₂O in 0.1 M TRIS-HCl-buffer (pH 7.4) were preincubated for 5 min at 37 °C and 750 rpm on a shaker. The reaction was started by adding the preheated compound at 1 mM resulting in a final concentration of 10 μM. The reaction was quenched at selected time points (0, 10, 20, 30, 60, and 120 min) by pipetting 100 μL of internal standard (ketoprofen) in acetonitrile at concentrations of 50 μM for compound **7B** and 35 μM for compound **13B**. The samples were vortexed for 30 s and centrifuged (21910 relative centrifugal force, 4 °C, 20 min). The supernatant was used directly for LC-MS analysis. All compound incubations were conducted at least in triplicates. Additionally, a negative control containing BSA (20 mg/mL) instead of liver microsomes and a positive control using Verapamil instead of compound were performed. A limit of 1% organic solvent during incubation was not exceeded. Sample separation and detection were performed on an *Alliance 2695 Separations Module* HPLC system (*Waters Corporation*, Milford, MA, USA) equipped with a *Phenomenex Kinetex 2.6 μm XB-C18 100 Å 50 x 3 mm* column (*Phenomenex Inc.*, Torrance, CA, USA) coupled to an *Alliance 2996 Photodiode Array Detector* and a *MICROMASS QUATTRO micro API* mass spectrometer (both *Waters Corporation*, Milford, MA, USA) using electrospray ionization in positive mode. Mobile phase A: 90% water, 10% acetonitrile and additionally 0.1% formic acid (v/v), mobile phase B: 100% acetonitrile with additionally 0.1% formic acid (v/v). The gradient was set to: 0-2.5 min 10% B, 2.5-10 min from 10 to 80% B, 10-12 min 80% B, 12-12.01 min from 80 to 10% B, 12.01-17 min 10% B at a flow rate of 0.7 mL/min. Samples were maintained at 10 °C, the column temperature was set to 20 °C with an injection volume of 5 μL. Spray, cone, extractor, and RF lens voltages were at 4 kV, 30 V, 8 V and 2 V, respectively. The source and desolvation temperatures were set to 120 °C and 350 °C, respectively, and the desolvation gas flow was set to 750 L/h. Data analysis was conducted using *MassLynx 4.1* software (*Waters Corporation*, Milford, MA, USA).

Glutathione (GSH) Stability Assay. The performed GSH stability assay for the compounds **7B**, **21**, **23**, **24** and the FDA-approved reference compound Afatinib was modified from a GSH assay established by Keeley et al. for analysis of heterocyclic electrophilic fragments [70, 26]. The following deviations from the original protocol were made: the reaction medium was changed to ACN/PBS-buffer 50:50 due to limited solubility of some compounds in aqueous buffer. After adding the buffer to the solution of the compounds in ACN the mixtures were filtered to avoid potential errors caused by compound precipitation. The reaction temperature was chosen to be 40 °C. The

reaction with GSH was monitored by measuring the decreasing area under the curve (AUC) of the compounds relative to the internal standard indoprofen.

Protein expression and purification. FGFR4 kinase domain (L445-E753) fused with a cleavable 6xHis affinity tag was expressed by BL21(DE3)-R3-lambda-PPase, which can co-express the lambda phosphatase to make the protein in a non-phosphorylated form. *E. coli* cells were cultured in TB medium supplemented with proper antibiotics at 37°C until OD₆₀₀ = 3, then induced with 0.5 mM isopropyl β-d-1-thiogalactopyranoside (IPTG), followed by overnight expression at 18°C at 180 rpm on a shaker. Cells were harvested and re-suspended in buffer: 50 mM HEPES at pH 7.5, 500 mM NaCl, 10 mM imidazole, 1 mM TCEP, 5% glycerol, then lysed by sonication on ice. The cell debris was removed by high-speed centrifuging and the supernatant was purified by immobilized metal affinity chromatography (IMAC) with Ni-sepharose resin (GE Healthcare) and the protein solution was passed through the Ni²⁺ beads again after the 6xHis affinity tag was cleaved. Size exclusion chromatography (SEC) was performed for further purification (protein in final buffer: 25 mM HEPES at pH 7.5, 250 mM NaCl, 0.5 mM TCEP, 5% glycerol). Protein concentration was measured by UV absorbance at A280 nm on a NanoDrop 2000 (Thermo Scientific) spectrophotometer, with the specific molar extinction coefficient and molecular weight of the target protein.

Intact protein MS. Protein concentration was adjusted to 50 μM and incubated with 100 μM of the covalent inhibitors **7A** and **7B** or non-reactive control **13B** at room temperature for 2 hours. The reaction was terminated by mixing with 1% formic acid in the ddH₂O, followed by desalting the sample with C8 stage tips according to the protocol previously described [71]. An injection volume of 5 μL was loaded for MS analysis. To remove protein carryover on the column, blank runs were performed between each sample injection. Acquisition of MS data was performed on Time-of-Flight (TOF) LC/MS (Agilent 6200 series) with positive electrospray ionization (ESI). Data were deconvoluted and analyzed by MassHunter Bioconfirm (Agilent), using 650-2000 m/z range, 10-100 KDa mass range, mass step of 1 Da and subtract baseline of 7.

Differential scanning fluorimetry (DSF) kinase panel. Differences in the melting temperature (ΔT_m) data were measured as described by Schwalm *et al* [72]. In brief: Purified proteins were buffered in 25 mM HEPES (pH 7.5) containing 500 mM NaCl and were assayed in a 384-wellplate with a final protein concentration of 2 μM in 10 μL

assay volume. Inhibitors were added to a final concentration of 20 μ M, using an ECHO 550 acoustic dispenser (Labcyte). As a fluorescence probe, SYPRO-Orange (Molecular Probes) was added in a 1:5000 dilution. Filters for excitation and emission were set to 465 nm and 590 nm, respectively. The temperature was increased from 25°C with 3°C/min to a final temperature of 95°C, while scanning, using the QuantStudio5 (Applied Biosystems). Data was analyzed through Boltzmann-equation in the Protein Thermal Shift software (Applied Biosystems). Samples were measured in technical duplicates.

NanoBRET assays. The assay was performed as described previously. [73] In brief: Full-length FGFR1-4 were obtained as plasmids cloned in frame with a terminal NanoLuc-fusion (kind gift from Promega). Plasmids were transfected into HEK293T cells using FuGENE HD (Promega, E2312) and proteins were allowed to express for 20 h. Serially diluted inhibitor and NanoBRET K10 Tracer (Promega, TracerDB ID: T000008) at the Tracer K_D concentration taken from TracerDB (tracerdb.org) were pipetted into white 384-well plates (Greiner 781207) using an ECHO acoustic dispenser (Labcyte). The corresponding protein-transfected cells were added and reseeded at a density of 2×10^5 cells/mL after trypsinization and resuspending in Opti-MEM without phenol red (Life Technologies). The system was allowed to equilibrate for 3 hours at 37°C/5% CO₂ prior to BRET measurements. To measure BRET, NanoBRET NanoGlo Substrate + extracellular NanoLuc Inhibitor (Promega, N2540) was added as per the manufacturer's protocol, and filtered luminescence was measured on a PHERAstar plate reader (BMG Labtech) equipped with a luminescence filter pair (450 nm BP filter (donor) and 610 nm LP filter (acceptor)). Competitive displacement data were then graphed using GraphPad Prism 9 software using a normalized 3-parameter curve fit with the following equation: $Y=100/(1+10^{(X-\text{LogIC}_{50})})$.

Acknowledgement

MK, RR, SL, DD and MG gratefully acknowledge the *Deutsche Forschungsgemeinschaft* (DFG, German Research Foundation) under Germany's excellence strategy – EXC 2180 – 390900677 [*Image Guided and Functionally Instructed Tumor Therapies*“ (iFIT)] for funding. MG further thanks the Deutsche

Forschungsgemeinschaft (DFG, German Research Foundation) – Project number 511101075, the Postdoctoral Fellowship Program of the Baden-Württemberg Stiftung and the Fonds der Chemischen Industrie (FCI) for financial support. SK, MPS and GW are grateful for funding by the Structural Genomics Consortium (SGC), a registered charity (no: 1097737) that receives funds from Bayer AG, Boehringer Ingelheim, Bristol Myers Squibb, Genentech, Genome Canada through Ontario Genomics Institute, EU/EFPIA/OICR/McGill/KTH/Diamond Innovative Medicines Initiative 2 Joint Undertaking [EUbOPEN grant 875510], Janssen, Merck KGaA, Pfizer and Takeda and by the German Cancer Research Center DKTK and the Frankfurt Cancer Institute (FCI). MPS is funded by the Deutsche Forschungsgemeinschaft (DFG, German Research Foundation), CRC1430 (Project-ID 424228829). Dr. Michael Forster, Dr. Stefan Gerstenecker and Lisa Haarer are acknowledged for fruitful discussion.

References

1. Dieci, M. V.; Arnedos, M.; Andre, F.; Soria, J. C. Fibroblast growth factor receptor inhibitors as a cancer treatment: from a biologic rationale to medical perspectives. *Cancer discovery* **2013**, *3* (3), 264–279. DOI: 10.1158/2159-8290.CD-12-0362.
2. Su, N.; Jin, M.; Chen, L. Role of FGF/FGFR signaling in skeletal development and homeostasis: learning from mouse models. *Bone research* **2014**, *2*, 14003. DOI: 10.1038/boneres.2014.3.
3. Itoh, N.; Ornitz, D. M. Fibroblast growth factors: from molecular evolution to roles in development, metabolism and disease. *Journal of biochemistry* **2011**, *149* (2), 121–130. DOI: 10.1093/jb/mvq121.
4. Eswarakumar, V. P.; Lax, I.; Schlessinger, J. Cellular signaling by fibroblast growth factor receptors. *Cytokine & growth factor reviews* **2005**, *16* (2), 139–149. DOI: 10.1016/j.cytogfr.2005.01.001.
5. Perera, T. P. S.; Jovcheva, E.; Mevellec, L.; Vialard, J.; Lange, D. de; Verhulst, T.; Paulussen, C.; van de Ven, K.; King, P.; Freyne, E.; Rees, D. C.; Squires, M.; Saxty, G.; Page, M.; Murray, C. W.; Gilissen, R.; Ward, G.; Thompson, N. T.; Newell, D. R.; Cheng, N.; Xie, L.; Yang, J.; Platero, S. J.; Karkera, J. D.; Moy, C.; Angibaud, P.; Laquerre, S.; Lorenzi, M. V. Discovery and Pharmacological Characterization of JNJ-42756493 (Erdafitinib), a Functionally Selective Small-Molecule FGFR Family Inhibitor. *Molecular cancer therapeutics* **2017**, *16* (6), 1010–1020. DOI: 10.1158/1535-7163.MCT-16-0589.
6. Wu, L.; Zhang, C.; He, C.; Qian, D.; Lu, L.; Sun, Y.; Xu, M.; Zhuo, J.; Liu, P. C. C.; Klabe, R.; Wynn, R.; Covington, M.; Gallagher, K.; Leffet, L.; Bowman, K.; Diamond, S.; Koblisch, H.; Zhang, Y.; Soloviev, M.; Hollis, G.; Burn, T. C.; Scherle, P.; Yeleswaram, S.; Huber, R.; Yao, W. Discovery of Pemigatinib: A Potent and Selective Fibroblast Growth Factor Receptor (FGFR) Inhibitor. *J. Med. Chem.* **2021**, *64* (15), 10666–10679. DOI: 10.1021/acs.jmedchem.1c00713.
7. Javle, M.; Roychowdhury, S.; Kelley, R. K.; Sadeghi, S.; Macarulla, T.; Weiss, K. H.; Waldschmidt, D.-T.; Goyal, L.; Borbath, I.; El-Khoueiry, A.; Borad, M. J.; Yong, W. P.; Philip, P. A.; Bitzer, M.; Tanasanvimon, S.; Li, A.; Pande, A.; Soifer, H. S.; Shepherd, S. P.; Moran, S.; Zhu, A. X.; Bekaii-Saab, T. S.; Abou-Alfa, G. K. Infigratinib (BGJ398) in previously treated patients with advanced or metastatic

- cholangiocarcinoma with FGFR2 fusions or rearrangements: mature results from a multicentre, open-label, single-arm, phase 2 study. *The lancet. Gastroenterology & hepatology* **2021**, *6* (10), 803–815. DOI: 10.1016/S2468-1253(21)00196-5.
8. Ito, S.; Otsuki, S.; Ohsawa, H.; Hirano, A.; Kazuno, H.; Yamashita, S.; Egami, K.; Shibata, Y.; Yamamiya, I.; Yamashita, F.; Kodama, Y.; Funabashi, K.; Kazuno, H.; Komori, T.; Suzuki, S.; Sootome, H.; Hirai, H.; Sagara, T. Discovery of Futibatinib: The First Covalent FGFR Kinase Inhibitor in Clinical Use. *ACS Med. Chem. Lett.* **2023**, *14* (4), 396–404. DOI: 10.1021/acsmchemlett.3c00006.
 9. Sung, H.; Ferlay, J.; Siegel, R. L.; Laversanne, M.; Soerjomataram, I.; Jemal, A.; Bray, F. Global Cancer Statistics 2020: GLOBOCAN Estimates of Incidence and Mortality Worldwide for 36 Cancers in 185 Countries. *CA: a cancer journal for clinicians* **2021**, *71* (3), 209–249. DOI: 10.3322/caac.21660.
 10. Kim, R. D.; Sarker, D.; Meyer, T.; Yau, T.; Macarulla, T.; Park, J.-W.; Choo, S. P.; Hollebecque, A.; Sung, M. W.; Lim, H.-Y.; Mazzaferro, V.; Trojan, J.; Zhu, A. X.; Yoon, J.-H.; Sharma, S.; Lin, Z.-Z.; Chan, S. L.; Faivre, S.; Feun, L. G.; Yen, C.-J.; Dufour, J.-F.; Palmer, D. H.; Llovet, J. M.; Manoojian, M.; Tugnait, M.; Stransky, N.; Hagel, M.; Kohl, N. E.; Lengauer, C.; Sherwin, C. A.; Schmidt-Kittler, O.; Hoeflich, K. P.; Shi, H.; Wolf, B. B.; Kang, Y.-K. First-in-Human Phase I Study of Fisogatinib (BLU-554) Validates Aberrant FGF19 Signaling as a Driver Event in Hepatocellular Carcinoma. *Cancer discovery* **2019**, *9* (12), 1696–1707. DOI: 10.1158/2159-8290.CD-19-0555.
 11. Poh, W.; Wong, W.; Ong, H.; Aung, M. O.; Lim, S. G.; Chua, B. T.; Ho, H. K. Klotho-beta overexpression as a novel target for suppressing proliferation and fibroblast growth factor receptor-4 signaling in hepatocellular carcinoma. *Molecular cancer* **2012**, *11*, 14. DOI: 10.1186/1476-4598-11-14.
 12. Vainikka, S.; Joukov, V.; Wennström, S.; Bergman, M.; Pelicci, P. G.; Alitalo, K. Signal transduction by fibroblast growth factor receptor-4 (FGFR-4). Comparison with FGFR-1. *Journal of Biological Chemistry* **1994**, *269* (28), 18320–18326. DOI: 10.1016/S0021-9258(17)32309-8.
 13. Kommalapati, A.; Tella, S. H.; Borad, M.; Javle, M.; Mahipal, A. FGFR Inhibitors in Oncology: Insight on the Management of Toxicities in Clinical Practice. *Cancers* **2021**, *13* (12). DOI: 10.3390/cancers13122968.

14. Dienstmann, R.; Rodon, J.; Prat, A.; Perez-Garcia, J.; Adamo, B.; Felip, E.; Cortes, J.; Iafrate, A. J.; Nuciforo, P.; Tabernero, J. Genomic aberrations in the FGFR pathway: opportunities for targeted therapies in solid tumors. *Annals of oncology : official journal of the European Society for Medical Oncology* **2014**, *25* (3), 552–563. DOI: 10.1093/annonc/mdt419.
15. Shimada, T.; Hasegawa, H.; Yamazaki, Y.; Muto, T.; Hino, R.; Takeuchi, Y.; Fujita, T.; Nakahara, K.; Fukumoto, S.; Yamashita, T. FGF-23 is a potent regulator of vitamin D metabolism and phosphate homeostasis. *Journal of bone and mineral research : the official journal of the American Society for Bone and Mineral Research* **2004**, *19* (3), 429–435. DOI: 10.1359/JBMR.0301264.
16. Wöhrle, S.; Bonny, O.; Beluch, N.; Gaulis, S.; Stamm, C.; Scheibler, M.; Müller, M.; Kinzel, B.; Thuery, A.; Brueggen, J.; Hynes, N. E.; Sellers, W. R.; Hofmann, F.; Graus-Porta, D. FGF receptors control vitamin D and phosphate homeostasis by mediating renal FGF-23 signaling and regulating FGF-23 expression in bone. *Journal of bone and mineral research : the official journal of the American Society for Bone and Mineral Research* **2011**, *26* (10), 2486–2497. DOI: 10.1002/jbmr.478.
17. Singh, J.; Petter, R. C.; Baillie, T. A.; Whitty, A. The resurgence of covalent drugs. *Nature reviews. Drug discovery* **2011**, *10* (4), 307–317. DOI: 10.1038/nrd3410.
18. Barf, T.; Kaptein, A. Irreversible protein kinase inhibitors: balancing the benefits and risks. *J. Med. Chem.* **2012**, *55* (14), 6243–6262. DOI: 10.1021/jm3003203.
19. Singh, J. The Ascension of Targeted Covalent Inhibitors. *J. Med. Chem.* **2022**, *65* (8), 5886–5901. DOI: 10.1021/acs.jmedchem.1c02134.
20. Serafim, R. A. M.; Elkins, J. M.; Zuercher, W. J.; Laufer, S. A.; Gehring, M. Chemical Probes for Understudied Kinases: Challenges and Opportunities. *J. Med. Chem.* **2022**, *65* (2), 1132–1170. DOI: 10.1021/acs.jmedchem.1c00980.
21. Serafim, R. A.; Haarer, L.; Pedreira, J. G.; Gehring, M. Covalent chemical probes for protein kinases. *Current Research in Chemical Biology* **2023**, *3*, 100040. DOI: 10.1016/j.crchbi.2022.100040.
22. Hillebrand, L.; Gehring, M. Never Gonna Give You Up - Current Developments in Covalent Protein Kinase Inhibitors. *Chimia* **2022**, *76* (5), 435–447. DOI: 10.2533/chimia.2022.435.

23. Gehring, M. Covalent Kinase Inhibitors: An Overview. In *Proteinkinase Inhibitors*; Laufer, S., Ed.; Topics in Medicinal Chemistry; Springer International Publishing, 2021, pp 43–94. DOI: 10.1007/7355_2020_103.
24. Nacht, M.; Qiao, L.; Sheets, M. P.; St Martin, T.; Labenski, M.; Mazdiyasni, H.; Karp, R.; Zhu, Z.; Chaturvedi, P.; Bhavsar, D.; Niu, D.; Westlin, W.; Petter, R. C.; Medikonda, A. P.; Singh, J. Discovery of a potent and isoform-selective targeted covalent inhibitor of the lipid kinase PI3K α . *J. Med. Chem.* **2013**, *56* (3), 712–721. DOI: 10.1021/jm3008745.
25. Borsari, C.; Keles, E.; McPhail, J. A.; Schaefer, A.; Sriramaratnam, R.; Goch, W.; Schaefer, T.; Pascale, M. de; Bal, W.; Gstaiger, M.; Burke, J. E.; Wymann, M. P. Covalent Proximity Scanning of a Distal Cysteine to Target PI3K α . *Journal of the American Chemical Society* **2022**, *144* (14), 6326–6342. DOI: 10.1021/jacs.1c13568.
26. Gerstenecker, S.; Haarer, L.; Schröder, M.; Kudolo, M.; Schwalm, M. P.; Wydra, V.; Serafim, R. A. M.; Chaikuad, A.; Knapp, S.; Laufer, S.; Gehring, M. Discovery of a Potent and Highly Isoform-Selective Inhibitor of the Neglected Ribosomal Protein S6 Kinase Beta 2 (S6K2). *Cancers* **2021**, *13* (20). DOI: 10.3390/cancers13205133.
27. Forster, M.; Gehring, M.; Laufer, S. A. Recent advances in JAK3 inhibition: Isoform selectivity by covalent cysteine targeting. *Bioorganic & medicinal chemistry letters* **2017**, *27* (18), 4229–4237. DOI: 10.1016/j.bmcl.2017.07.079.
28. Telliez, J.-B.; Dowty, M. E.; Wang, L.; Jussif, J.; Lin, T.; Li, L.; Moy, E.; Balbo, P.; Li, W.; Zhao, Y.; Crouse, K.; Dickinson, C.; Symanowicz, P.; Hegen, M.; Banker, M. E.; Vincent, F.; Unwalla, R.; Liang, S.; Gilbert, A. M.; Brown, M. F.; Hayward, M.; Montgomery, J.; Yang, X.; Bauman, J.; Trujillo, J. I.; Casimiro-Garcia, A.; Vajdos, F. F.; Leung, L.; Geoghegan, K. F.; Quazi, A.; Xuan, D.; Jones, L.; Hett, E.; Wright, K.; Clark, J. D.; Thorarensen, A. Discovery of a JAK3-Selective Inhibitor: Functional Differentiation of JAK3-Selective Inhibition over pan-JAK or JAK1-Selective Inhibition. *ACS chemical biology* **2016**, *11* (12), 3442–3451. DOI: 10.1021/acscchembio.6b00677.
29. Thorarensen, A.; Dowty, M. E.; Banker, M. E.; Juba, B.; Jussif, J.; Lin, T.; Vincent, F.; Czerwinski, R. M.; Casimiro-Garcia, A.; Unwalla, R.; Trujillo, J. I.; Liang, S.; Balbo, P.; Che, Y.; Gilbert, A. M.; Brown, M. F.; Hayward, M.; Montgomery, J.;

- Leung, L.; Yang, X.; Soucy, S.; Hegen, M.; Coe, J.; Langille, J.; Vajdos, F.; Chrencik, J.; Telliez, J.-B. Design of a Janus Kinase 3 (JAK3) Specific Inhibitor 1-((2S,5R)-5-((7H-Pyrrolo[2,3-d]pyrimidin-4-yl)amino)-2-methylpiperidin-1-yl)prop-2-en-1-one (PF-06651600) Allowing for the Interrogation of JAK3 Signaling in Humans. *J. Med. Chem.* **2017**, *60* (5), 1971–1993. DOI: 10.1021/acs.jmedchem.6b01694.
30. Fairhurst, R. A.; Knoepfel, T.; Leblanc, C.; Buschmann, N.; Gaul, C.; Blank, J.; Galuba, I.; Trappe, J.; Zou, C.; Voshol, J.; Genick, C.; Brunet-Lefeuvre, P.; Bitsch, F.; Graus-Porta, D.; Furet, P. Approaches to selective fibroblast growth factor receptor 4 inhibition through targeting the ATP-pocket middle-hinge region. *MedChemComm* **2017**, *8* (8), 1604–1613. DOI: 10.1039/c7md00213k.
31. Chaikuad, A.; Koch, P.; Laufer, S. A.; Knapp, S. The Cysteine of Protein Kinases as a Target in Drug Development. *Angewandte Chemie (International ed. in English)* **2018**, *57* (16), 4372–4385. DOI: 10.1002/anie.201707875.
32. Hagel, M.; Miduturu, C.; Sheets, M.; Rubin, N.; Weng, W.; Stransky, N.; Bifulco, N.; Kim, J. L.; Hodous, B.; Brooijmans, N.; Shutes, A.; Winter, C.; Lengauer, C.; Kohl, N. E.; Guzi, T. First Selective Small Molecule Inhibitor of FGFR4 for the Treatment of Hepatocellular Carcinomas with an Activated FGFR4 Signaling Pathway. *Cancer discovery* **2015**, *5* (4), 424–437. DOI: 10.1158/2159-8290.CD-14-1029.
33. Zhong, Z.; Shi, L.; Fu, T.; Huang, J.; Pan, Z. Discovery of Novel 7-Azaindole Derivatives as Selective Covalent Fibroblast Growth Factor Receptor 4 Inhibitors for the Treatment of Hepatocellular Carcinoma. *Journal of medicinal chemistry* **2022**, *65* (10), 7278–7295. DOI: 10.1021/acs.jmedchem.2c00255.
34. Zhang, X.; Wang, Y.; Ji, J.; Si, D.; Bao, X.; Yu, Z.; Zhu, Y.; Zhao, L.; Li, W.; Liu, J. Discovery of 1,6-Naphthyridin-2(1H)-one Derivatives as Novel, Potent, and Selective FGFR4 Inhibitors for the Treatment of Hepatocellular Carcinoma. *J. Med. Chem.* **2022**, *65* (11), 7595–7618. DOI: 10.1021/acs.jmedchem.1c01977.
35. Shao, M.; Chen, X.; Yang, F.; Song, X.; Zhou, Y.; Lin, Q.; Fu, Y.; Ortega, R.; Lin, X.; Tu, Z.; Patterson, A. V.; Smaill, J. B.; Chen, Y.; Lu, X. Design, Synthesis, and Biological Evaluation of Aminoindazole Derivatives as Highly Selective Covalent Inhibitors of Wild-Type and Gatekeeper Mutant FGFR4. *J. Med. Chem.* **2022**, *65* (6), 5113–5133. DOI: 10.1021/acs.jmedchem.2c00096.

36. Deng, W.; Chen, X.; Jiang, K.; Song, X.; Huang, M.; Tu, Z.-C.; Zhang, Z.; Lin, X.; Ortega, R.; Patterson, A. V.; Smaill, J. B.; Ding, K.; Chen, S.; Chen, Y.; Lu, X. Investigation of Covalent Warheads in the Design of 2-Aminopyrimidine-based FGFR4 Inhibitors. *ACS Med. Chem. Lett.* **2021**, *12* (4), 647–652. DOI: 10.1021/acsmchemlett.1c00052.
37. Nie, W.; Lu, Y.; Pan, C.; Gao, J.; Luo, M.; Du, J.; Wang, J.; Luo, P.; Zhu, H.; Che, J.; He, Q.; Dong, X. Design, synthesis, and biological evaluation of quinazoline derivatives with covalent reversible warheads as potential FGFR4 inhibitors. *Bioorganic chemistry* **2022**, *121*, 105673. DOI: 10.1016/j.bioorg.2022.105673.
38. Pan, C.; Nie, W.; Wang, J.; Du, J.; Pan, Z.; Gao, J.; Lu, Y.; Che, J.; Zhu, H.; Dai, H.; Chen, B.; He, Q.; Dong, X. Design, synthesis and biological evaluation of quinazoline derivatives as potent and selective FGFR4 inhibitors. *European journal of medicinal chemistry* **2021**, *225*, 113794. DOI: 10.1016/j.ejmech.2021.113794.
39. Zhou, M.; Zhu, S.; Xu, C.; Liu, B.; Shen, J. A phase Ib/II study of BLU-554, a fibroblast growth factor receptor 4 inhibitor in combination with CS1001, an anti-PD-L1, in patients with locally advanced or metastatic hepatocellular carcinoma. *Investigational new drugs* **2023**, *41* (1), 162–167. DOI: 10.1007/s10637-023-01335-w.
40. Macarulla, T.; Moreno, V.; Chen, L.-T.; Sawyer, M. B.; Goyal, L.; Muñoz Martín, A. J.; Sheng-Shun, Y.; Le Sourd, S.; Morris, J.; Fuchs, M.; Karasic, T. B.; Kang, Y.-K.; Yong, W.-P.; Selvaraj, A.; Destenaves, B.; Xiao, J. A.; Gomez, R.; Gualberto, A.; Pipas, J. M. M.; Finn, R. S. Phase I study of H3B-6527 in hepatocellular carcinoma (HCC) or intrahepatic cholangiocarcinoma (ICC). *JCO* **2021**, *39* (15_suppl), 4090. DOI: 10.1200/JCO.2021.39.15_suppl.4090.
41. Joshi, J. J.; Coffey, H.; Corcoran, E.; Tsai, J.; Huang, C.-L.; Ichikawa, K.; Prajapati, S.; Hao, M.-H.; Bailey, S.; Wu, J.; Rimkunas, V.; Karr, C.; Subramanian, V.; Kumar, P.; MacKenzie, C.; Hurley, R.; Satoh, T.; Yu, K.; Park, E.; Rioux, N.; Kim, A.; Lai, W. G.; Yu, L.; Zhu, P.; Buonamici, S.; Larsen, N.; Fekkes, P.; Wang, J.; Warmuth, M.; Reynolds, D. J.; Smith, P. G.; Selvaraj, A. H3B-6527 Is a Potent and Selective Inhibitor of FGFR4 in FGF19-Driven Hepatocellular Carcinoma. *Cancer research* **2017**, *77* (24), 6999–7013. DOI: 10.1158/0008-5472.CAN-17-1865.

42. Knoepfel, T.; Furet, P.; Mah, R.; Buschmann, N.; Leblanc, C.; Ripoché, S.; Graus-Porta, D.; Wartmann, M.; Galuba, I.; Fairhurst, R. A. 2-Formylpyridyl Ureas as Highly Selective Reversible-Covalent Inhibitors of Fibroblast Growth Factor Receptor 4. *ACS Med. Chem. Lett.* **2018**, *9* (3), 215–220. DOI: 10.1021/acsmchemlett.7b00485.
43. Yang, F.; Chen, X.; Song, X.; Ortega, R.; Lin, X.; Deng, W.; Guo, J.; Tu, Z.; Patterson, A. V.; Smail, J. B.; Chen, Y.; Lu, X. Design, Synthesis, and Biological Evaluation of 5-Formyl-pyrrolo[3,2-b]pyridine-3-carboxamides as New Selective, Potent, and Reversible-Covalent FGFR4 Inhibitors. *Journal of medicinal chemistry* **2022**, *65* (21), 14809–14831. DOI: 10.1021/acs.jmedchem.2c01319.
44. Zhang, Z.; Li, J.; Chen, H.; Huang, J.; Song, X.; Tu, Z.-C.; Zhang, Z.; Peng, L.; Zhou, Y.; Ding, K. Design, Synthesis, and Biological Evaluation of 2-Formyl Tetrahydronaphthyridine Urea Derivatives as New Selective Covalently Reversible FGFR4 Inhibitors. *J. Med. Chem.* **2022**, *65* (4), 3249–3265. DOI: 10.1021/acs.jmedchem.1c01816.
45. Fairhurst, R. A.; Knoepfel, T.; Buschmann, N.; Leblanc, C.; Mah, R.; Todorov, M.; Nimsgern, P.; Ripoché, S.; Niklaus, M.; Warin, N.; van Luu, H.; Madoerin, M.; Wirth, J.; Graus-Porta, D.; Weiss, A.; Kiffe, M.; Wartmann, M.; Kinyamu-Akunda, J.; Sterker, D.; Stamm, C.; Adler, F.; Buhles, A.; Schadt, H.; Couttet, P.; Blank, J.; Galuba, I.; Trappe, J.; Voshol, J.; Ostermann, N.; Zou, C.; Berghausen, J.; Del Rio Espinola, A.; Jahnke, W.; Furet, P. Discovery of Roblitinib (FGF401) as a Reversible-Covalent Inhibitor of the Kinase Activity of Fibroblast Growth Factor Receptor 4. *J. Med. Chem.* **2020**, *63* (21), 12542–12573. DOI: 10.1021/acs.jmedchem.0c01019.
46. Faridooon; Ng, R.; Zhang, G.; Li, J. J. An update on the discovery and development of reversible covalent inhibitors. *Medicinal chemistry research : an international journal for rapid communications on design and mechanisms of action of biologically active agents* **2023**, *32* (6), 1039–1062. DOI: 10.1007/s00044-023-03065-3.
47. Gehringer, M.; Laufer, S. A. Emerging and Re-Emerging Warheads for Targeted Covalent Inhibitors: Applications in Medicinal Chemistry and Chemical Biology. *Journal of medicinal chemistry* **2019**, *62* (12), 5673–5724. DOI: 10.1021/acs.jmedchem.8b01153.

48. Malona, J.; Chuaqui, C.; Seletsky, B. M.; Beebe, L.; Cantin, S.; van Kalken, D.; Fahnoe, K.; Wang, Z.; Browning, B.; Szabo, H.; Koopman, L. A.; Oravec, T.; McDonald, J. J.; Ramirez-Valle, F.; Gaur, R.; Mensah, K. A.; Thomas, M.; Connarn, J. N.; Hu, H.; Alexander, M. D.; Corin, A. F. Discovery of CC-99677, a selective targeted covalent MAPKAPK2 (MK2) inhibitor for autoimmune disorders. *Translational research : the journal of laboratory and clinical medicine* **2022**, *249*, 49–73. DOI: 10.1016/j.trsl.2022.06.005.
49. Wydra, V.; Gerstenecker, S.; Schollmeyer, D.; Andreev, S.; Dimitrov, T.; Massarico Serafim, R. A.; Laufer, S.; Gehringer, M. N-(6-Chloro-3-nitropyridin-2-yl)-5-(1-methyl-1H-pyrazol-4-yl)isoquinolin-3-amine. *Molbank* **2021**, *2021* (1), M1181. DOI: 10.3390/M1181.
50. Zheng, J.; Zhang, W.; Li, L.; He, Y.; Wei, Y.; Dang, Y.; Nie, S.; Guo, Z. Signaling Pathway and Small-Molecule Drug Discovery of FGFR: A Comprehensive Review. *Frontiers in chemistry* **2022**, *10*, 860985. DOI: 10.3389/fchem.2022.860985.
51. Qu, L.; Chen, X.; Wei, H.; Guo, M.; Dai, S.; Jiang, L.; Li, J.; Yue, S.; Chen, Z.; Chen, Y. Structural insights into the potency and selectivity of covalent pan-FGFR inhibitors. *Communications chemistry* **2022**, *5* (1), 5. DOI: 10.1038/s42004-021-00623-x.
52. Xing, L.; Klug-Mcleod, J.; Rai, B.; Lunney, E. A. Kinase hinge binding scaffolds and their hydrogen bond patterns. *Bioorganic & medicinal chemistry* **2015**, *23* (19), 6520–6527. DOI: 10.1016/j.bmc.2015.08.006.
53. Bruno, N. C.; Tudge, M. T.; Buchwald, S. L. Design and Preparation of New Palladium Precatalysts for C-C and C-N Cross-Coupling Reactions. *Chemical science* **2013**, *4*, 916–920. DOI: 10.1039/C2SC20903A.
54. Wittlinger, F.; Heppner, D. E.; To, C.; Günther, M.; Shin, B. H.; Rana, J. K.; Schmoker, A. M.; Beyett, T. S.; Berger, L. M.; Berger, B.-T.; Bauer, N.; Vasta, J. D.; Corona, C. R.; Robers, M. B.; Knapp, S.; Jänne, P. A.; Eck, M. J.; Laufer, S. A. Design of a "Two-in-One" Mutant-Selective Epidermal Growth Factor Receptor Inhibitor That Spans the Orthosteric and Allosteric Sites. *J. Med. Chem.* **2022**, *65* (2), 1370–1383. DOI: 10.1021/acs.jmedchem.1c00848.
55. Neil Bifulco, Jr. Natasja Brooijmans Brian L. Hodous Joseph L. Kim Chandrasekhar V. MIDUTURU. Inhibitors of the fibroblast growth factor receptor.

56. Bennani, Y. L.; Hanessian, S. trans-1,2-Diaminocyclohexane Derivatives as Chiral Reagents, Scaffolds, and Ligands for Catalysis: Applications in Asymmetric Synthesis and Molecular Recognition. *Chemical reviews* **1997**, *97* (8), 3161–3196. DOI: 10.1021/cr9407577.
57. Morales-Colón, M. T.; See, Y. Y.; Lee, S. J.; Scott, P. J. H.; Bland, D. C.; Sanford, M. S. Tetramethylammonium Fluoride Alcohol Adducts for SNAr Fluorination. *Organic letters* **2021**, *23* (11), 4493–4498. DOI: 10.1021/acs.orglett.1c01490.
58. Schlosser, M.; Cottet, F. Silyl-Mediated Halogen/Halogen Displacement in Pyridines and Other Heterocycles. *Eur. J. Org. Chem.* **2002**, *2002* (24), 4181–4184. DOI: 10.1002/1099-0690(200212)2002:24<4181:AID-EJOC4181>3.0.CO;2-M.
59. Ishiyama, T.; Murata, M.; Miyaura, N. Palladium(0)-Catalyzed Cross-Coupling Reaction of Alkoxydiboron with Haloarenes: A Direct Procedure for Arylboronic Esters. *J. Org. Chem.* **1995**, *60* (23), 7508–7510. DOI: 10.1021/jo00128a024.
60. Anastassiadis, T.; Deacon, S. W.; Devarajan, K.; Ma, H.; Peterson, J. R. Comprehensive assay of kinase catalytic activity reveals features of kinase inhibitor selectivity. *Nature biotechnology* **2011**, *29* (11), 1039–1045. DOI: 10.1038/nbt.2017.
61. Luković, E.; González-Vera, J. A.; Imperiali, B. Recognition-domain focused chemosensors: versatile and efficient reporters of protein kinase activity. *Journal of the American Chemical Society* **2008**, *130* (38), 12821–12827. DOI: 10.1021/ja8046188.
62. Hatlen, M. A.; Schmidt-Kittler, O.; Sherwin, C. A.; Rozsahegyi, E.; Rubin, N.; Sheets, M. P.; Kim, J. L.; Miduturu, C.; Bifulco, N.; Brooijmans, N.; Shi, H.; Guzi, T.; Boral, A.; Lengauer, C.; Dorsch, M.; Kim, R. D.; Kang, Y.-K.; Wolf, B. B.; Hoeflich, K. P. Acquired On-Target Clinical Resistance Validates FGFR4 as a Driver of Hepatocellular Carcinoma. *Cancer discovery* **2019**, *9* (12), 1686–1695. DOI: 10.1158/2159-8290.CD-19-0367.
63. Lo, M.-C.; Aulabaugh, A.; Jin, G.; Cowling, R.; Bard, J.; Malamas, M.; Ellestad, G. Evaluation of fluorescence-based thermal shift assays for hit identification in drug discovery. *Analytical Biochemistry* **2004**, *332* (1), 153–159. DOI: 10.1016/j.ab.2004.04.031.

64. Ciceri, P.; Müller, S.; O'Mahony, A.; Fedorov, O.; Filippakopoulos, P.; Hunt, J. P.; Lasater, E. A.; Pallares, G.; Picaud, S.; Wells, C.; Martin, S.; Wodicka, L. M.; Shah, N. P.; Treiber, D. K.; Knapp, S. Dual kinase-bromodomain inhibitors for rationally designed polypharmacology. *Nature chemical biology* **2014**, *10* (4), 305–312. DOI: 10.1038/nchembio.1471.
65. Laufer, S.; Bajorath, J.; Gehring, M.; Gray, N.; Frye, S.; Lindsley, C. W. Publication Criteria and Requirements for Studies on Protein Kinase Inhibitors—What Is Expected? *J. Med. Chem.* **2022**, *65* (10), 6973–6974. DOI: 10.1021/acs.jmedchem.2c00623.
66. Hartung, I. V.; Rudolph, J.; Mader, M. M.; Mulder, M. P. C.; Workman, P. Expanding Chemical Probe Space: Quality Criteria for Covalent and Degradable Probes. *J. Med. Chem.* **2023**, *66* (14), 9297–9312. DOI: 10.1021/acs.jmedchem.3c00550.
67. Hoyt, K. W.; Urul, D. A.; Ogboo, B. C.; Wittlinger, F.; Laufer, S. A.; Schaefer, E. M.; May, E. W.; Heppner, D. E. Pitfalls and Considerations in Determining the Potency and Mutant Selectivity of Covalent Epidermal Growth Factor Receptor Inhibitors. *J. Med. Chem.* **2023**. DOI: 10.1021/acs.jmedchem.3c01502.
68. Schwartz, P. A.; Kuzmic, P.; Solowiej, J.; Bergqvist, S.; Bolanos, B.; Almaden, C.; Nagata, A.; Ryan, K.; Feng, J.; Dalvie, D.; Kath, J. C.; Xu, M.; Wani, R.; Murray, B. W. Covalent EGFR inhibitor analysis reveals importance of reversible interactions to potency and mechanisms of drug resistance. *Proceedings of the National Academy of Sciences of the United States of America* **2014**, *111* (1), 173–178. DOI: 10.1073/pnas.1313733111.
69. Zhai, X.; Ward, R. A.; Doig, P.; Argyrou, A. Insight into the Therapeutic Selectivity of the Irreversible EGFR Tyrosine Kinase Inhibitor Osimertinib through Enzyme Kinetic Studies. *Biochemistry* **2020**, *59* (14), 1428–1441. DOI: 10.1021/acs.biochem.0c00104.
70. Keeley, A.; Ábrányi-Balogh, P.; Keserű, G. M. Design and characterization of a heterocyclic electrophilic fragment library for the discovery of cysteine-targeted covalent inhibitors. *MedChemComm* **2019**, *10* (2), 263–267. DOI: 10.1039/C8MD00327K.
71. Rappsilber, J.; Ishihama, Y.; Mann, M. Stop and go extraction tips for matrix-assisted laser desorption/ionization, nanoelectrospray, and LC/MS sample

pretreatment in proteomics. *Analytical chemistry* **2003**, *75* (3), 663–670. DOI: 10.1021/ac026117i.

72. Schwalm, M. P.; Berger, L. M.; Meuter, M. N.; Vasta, J. D.; Corona, C. R.; Röhm, S.; Berger, B.-T.; Farges, F.; Beinert, S. M.; Preuss, F.; Morasch, V.; Rogov, V. V.; Mathea, S.; Saxena, K.; Robers, M. B.; Müller, S.; Knapp, S. A Toolbox for the Generation of Chemical Probes for Baculovirus IAP Repeat Containing Proteins. *Frontiers in cell and developmental biology* **2022**, *10*, 886537. DOI: 10.3389/fcell.2022.886537.

73. Schwalm, M. P.; Krämer, A.; Dölle, A.; Weckesser, J.; Yu, X.; Jin, J.; Saxena, K.; Knapp, S. Tracking the PROTAC degradation pathway in living cells highlights the importance of ternary complex measurement for PROTAC optimization. *Cell chemical biology* **2023**, *30* (7), 753-765.e8. DOI: 10.1016/j.chembiol.2023.06.002.